JOURNAL OF GEOPHYSICAL RESEARCH, VOL. 100, NO. C5, PAGES 8501–8522, MAY 15, 1995

An ocean large-eddy simulation of Langmuir circulations and convection in the surface mixed layer

Eric D. Skyllingstad and Donald W. Denbo
Pacific Northwest Laboratory, Sequim, Washington

Abstract. Numerical experiments were performed using a three-dimensional large-eddy simulation model of the ocean surface mixed layer that includes the Craik-Leibovich vortex force [*Craik* 1977; *Leibovich* 1977] to parameterize the interaction of surface waves with mean currents. Results from the experiments show that the vortex force generates Langmuir circulations that can dominate vertical mixing. The simulated vertical velocity fields show linear, small-scale, coherent structures near the surface that extend downwind across the model domain. In the interior of the mixed layer, scales of motion increase to eddy sizes that are roughly equivalent to the mixed-layer depth. Cases with the vortex force have stronger circulations near the surface in contrast to cases with only heat flux and wind stress, particularly when the heat flux is positive. Calculations of the velocity variance and turbulence dissipation rates for cases with and without the vortex force, surface cooling, and wind stress indicate that wave-current interactions are a dominant mixing process in the upper mixed layer. Heat flux calculations show that the entrainment rate at the mixed-layer base can be up to two times greater when the vortex force is included. In a case with reduced wind stress, turbulence dissipation rates remained high near the surface because of the vortex force interaction with preexisting inertial currents. In deep mixed layers (~250 m) the simulations show that Langmuir circulations can vertically transport water 145 m during conditions of surface heating. Observations of turbulence dissipation rates and the vertical temperature structure support the model results.

1. Introduction

Mixing in the ocean surface layer is an important process in the transport of heat, momentum, and trace chemicals from the atmosphere to the interior ocean and may play a significant role in determining the climatic behavior of the global ocean circulation. For example, numerical simulations of the global ocean using ocean general circulation models (OGCMs) have shown that the thermohaline circulation depends greatly on the type of surface boundary forcing and on the strength of vertical diffusive mixing [*Bryan,* 1987; *Cummins et al.,* 1990; *Gargett and Holloway,* 1992; *Tziperman et al.,* 1994]. The dynamics of the ocean surface layer differ from the bulk of the ocean circulation, because the layer is frequently well mixed and dominated by relatively small-scale motions. Processes thought to govern the structure of the ocean boundary layer include convection forced from nighttime cooling, shear stress instability generated by surface wind stress, and circulations resulting from interaction of surface waves with wind-driven currents. The action of these processes can be divided into buoyancy-dominated and wind-dominated circulations. With weak winds and strong cooling the surface mixed layer behaves like a convective boundary layer with characteristic scales that are consistent with similarity theory [*Lombardo and Gregg,* 1989; *Shay and Gregg,* 1986]. When wind forcing dominates, turbulence is generated by shear instability and by coherent roll vortices, known as Langmuir circulations, that form in response to wave-current interactions [*Leibovich,* 1983]. In this paper we investigate the importance of wind- versus buoyancy-forced motions by modeling the ocean surface layer with a large-eddy simulation (LES) model modified to include effects of wave-current interaction. Our goal is to gain a better understanding of mixing processes in the surface layer and to aid in the design of a more accurate mixed-layer parameterization for OGCMs.

Ocean surface layer bulk properties during convective conditions with weak wind forcing strongly resemble an atmospheric convective boundary layer. In particular, *Shay and Gregg* [1986] and *Lombardo and Gregg* [1989] showed that turbulence dissipation rates scale according to similarity theory values under conditions of surface cooling and moderate surface wind stress. Furthermore, they observed a diurnal cycle of the boundary layer depth like that of the atmosphere (but reversed in time), with entrainment growth at night during convection and collapse of turbulence at sunrise, when the ocean surface layer restratifies. There is also evidence that the convective ocean boundary layer has a three-layer structure similar to that of the atmosphere [*Anis and Moum,* 1992]. The layers are divided into a microlayer near the surface where molecular processes dominate, a surface layer where turbulent fluxes of momentum and heat are constant with depth, and a mixed layer where the motions are dominated by large-scale convective plumes.

The most significant difference between the ocean and atmosphere boundary layers is evident when wind stress and surface waves are present, particularly when the surface heat flux is stabilizing. Wind stress acting on the ocean surface generates a vertically sheared horizontal current and surface

Paper number 94JC03202.
0148-0227/95/94JC-03202$05.00

gravity waves, which can interact to produce Langmuir circulations [*Leibovich*, 1983]. Turbulence enhanced by these circulations, along with surface wave breaking, leads to increased turbulence dissipation that can exceed similarity scales by as much as a factor of 10 in the upper one third of the mixed layer [*Anis and Moum*, 1992].

Observations of Langmuir circulations show a wide range of scales and intensities. *Smith et al.* [1987] and *Weller et al.* [1985] observed circulations off the coast of California having vertical and horizontal velocities exceeding 0.25 m s^{-1}, surface convergence lines extending up to 2 km in length, and convergence cells with separations ranging from 120 to 180 m. More recently, *Smith* [1992] described acoustic Doppler velocity measurements off the coast of California that showed the growth of Langmuir circulations with downwelling velocities of roughly 0.1 m s^{-1} in response to an increase in surface wind speed from 8 to 13 m s^{-1}. Smith's analysis indicated an aspect ratio of about 1 for the spacing and depth of the Langmuir circulation cells, in contrast to the 1.5 to 3.0 estimate given by *Smith et al.* [1987]. Measurements with side-scan sonar of bubble plumes in a lake indicate a similar structure with a range of Langmuir cell separation [*Thorpe*, 1992]. The observed bubble plumes were characterized by streaks of various scales that merge to form the main circulation cells. The streaks were frequently aligned downwind and propagated to the right of the mean wind direction, implying a Coriolis effect or Ekman drift. A summary of earlier field observations of Langmuir circulations is given by *Leibovich* [1983].

The prevailing theory for Langmuir circulations is that of *Craik* [1977] and *Leibovich* [1977], referred to as the CL2 model [*Faller and Caponi*, 1978], which describes the formation of Langmuir circulations in terms of an instability brought on by the interaction of the wave Stokes drift with the wind-driven surface shear current. The instability is initiated by a "vortex force" term that appears in the right-hand side of the momentum equations as

$$\vec{V}_s \times \vec{\omega} \tag{1}$$

where $\vec{V}_s$ is the Stokes drift velocity and $\vec{\omega}$ is the vorticity. This term acts like a buoyancy force in the vertical equation of motion, but with a directional dependency that follows the Stokes drift. The CL2 theory predicts circulations with all of the qualitative features of Langmuir circulations as outlined by *Craik and Leibovich* [1976], namely, wind-driven vortices parallel to the wind direction, asymmetric structure with downwelling regions smaller than upwelling regions, downwelling zones under maximum surface drift current regions, and maximum downwelling speeds comparable to the surface current speed.

Application of the CL2 model has, in general, been limited to two-dimensional applications that do not allow along-wind variability. Because of these simplifications, theoretical studies of Langmuir circulations have not shown the range of scales in wavelength and along-wind variation that appear in the measurements. For example, using the two-dimensional CL2 equations, *Li and Garrett* [1993] were able to model cell merging but could not simulate the regeneration of small-scale cells, as observed by *Weller and Price* [1988]. Spatial variations in the velocity and surface convergence, as reported by *Weller et al.* [1985] and *Smith et al.* [1987], cannot be effectively examined without considering the full, three-dimensional structure of the circulations. *Leibovich and Tandon* [1993] addressed part of this problem by applying a semianalytical solution to the three-dimensional linearized CL2 model, showing that stratification causes the most unstable Langmuir modes to be three-dimensional with a cross-stream orientation. However, they could not examine finite-amplitude behavior of Langmuir circulations because of the linear assumption on the CL2 equations. General, three-dimensional, nonlinear interactions of Langmuir circulations with sheared currents and other convectively driven structures have not been studied. These interactions may lead to the range of scales and bifurcations noted in observations.

To address these problems and extend the use of the CL2 model, we modified a three-dimensional LES model by adding the vortex force given in (1) as a wave-current interaction parameterization. Details of the CL2 modification are described in section 2, and a brief overview of the LES model is given. We examined the effects of surface forcing on the ocean mixed layer by applying the modified LES model in a series of process experiments. These experiments are motivated by the need for a better understanding of how wind, waves, and surface heating generate mixing in the ocean surface layer. Because we are mainly interested in the physics of these processes, idealized initial conditions and surface boundary conditions were used throughout the study.

The results of these process experiments are presented in section 3. We show that the ocean mixed layer is strongly affected by wave-current interaction, particularly when conditions favor stratification (i.e., strong solar heating). For example, application of a typical diurnal cycle of heating and a constant wind and wave field produces aligned cellular convection at night and Langmuir-like circulations during the day. When wind and wave forcing is removed, the model generates a less energetic convective boundary layer at night and a strongly stratified, shallow surface layer during the day. Comparison of model-derived statistics shows that the addition of the vortex force leads to a downwind shift in the peak wavenumber and an increase in the eddy activity and turbulence dissipation rate near the surface. Moreover, the combination of Langmuir circulations and buoyant convection causes an increase in the mixed-layer entrainment rate by as much as a factor of 2 over the individual process entrainment rates predicted by the model. Experiments with high-latitude, wintertime surface forcing show that Langmuir circulations are capable of transporting water to depths greater than 145 m during extreme winter storm conditions. This result is important because of the principal role Langmuir circulations may play in eroding the seasonal thermocline.

2. Description of the Model

LES models are designed to resolve the largest turbulent motions in geophysical boundary layer problems. These models typically resolve a portion of the Kolmogorov inertial subrange where the spectral energy decreases proportionally to $k^{-5/3}$, where k is the horizontal wavenumber [*Kaimal and Finnigan*, 1994; *Mason*, 1994]. Comparison of LES results from the atmospheric boundary layer have shown that these models are capable of accurately simulating many of the observed features and statistics of atmospheric turbulence

[*Wyngaard*, 1992]. Preliminary LES results for the ocean (without surface wave effects) also yield a boundary layer that is consistent with atmospheric observations [*McWilliams*, 1993]. The LES model used in this study is based on the nonhydrostatic, Boussinesq equations described by *Deardorff* [1980], with improvements in the numerical solution techniques. A complete description of the model is presented D.W. Denbo and E.D. Skyllingstad (An ocean large eddy model with application to deep convection in the Greenland Sea, submitted to *Journal of Geophysical Research*, 1994), along with validation experiment results.

Three modifications of the model were made specifically for this study to account for the radiation of internal wave energy through the model bottom and to include the CL2 vortex force term for wave-current interaction. The bottom-boundary radiation condition is based on a scheme developed by *Klemp and Durran* [1983] for the top boundary of atmospheric models. The scheme prescribes the lower-boundary pressure based on a relationship between vertical velocity and pressure for linear internal gravity waves. This relationship defines the correct pressure field that would exist if the internal waves propagated without reflection. As shown by Klemp and Durran, the scheme is very robust for low-amplitude disturbances in weak shear. In this study the bottom boundary is typically located within the permanent thermocline and far enough below the mixed layer to preclude strong shear or internal wave activity.

The momentum equations were modified by including the vortex force for each component of the velocity field,

$$\frac{\partial u}{\partial t} = -\frac{1}{\rho_\circ}\frac{\partial P}{\partial x} + R_u + v_s\left(\frac{\partial v}{\partial x} - \frac{\partial u}{\partial y}\right),$$

$$\frac{\partial v}{\partial t} = -\frac{1}{\rho_\circ}\frac{\partial P}{\partial y} + R_v + u_s\left(\frac{\partial u}{\partial y} - \frac{\partial v}{\partial x}\right),$$

$$\frac{\partial w}{\partial t} = -\frac{1}{\rho_\circ}\frac{\partial P}{\partial z} + R_w + u_s\left(\frac{\partial u}{\partial z} - \frac{\partial w}{\partial x}\right) + v_s\left(\frac{\partial v}{\partial z} - \frac{\partial w}{\partial y}\right), \quad (2)$$

where u, v, and w and x, y, and z are the zonal, meridional, and vertical velocity components and directions, respectively; t is time; ρ_o is the average density; P is a modified pressure; R_u, R_v, and R_w represent the combined advection, Coriolis, and subgrid-scale mixing terms for each velocity component; and u_s and v_s are the zonal and meridional Stokes drift components. These terms are cast in finite difference form using centered differences consistent with the leapfrog time differencing. We also included the effect of the Stokes drift on the transport of scalar fields (i.e., temperature, salinity, and subgrid-scale turbulent kinetic energy) by adding the Stokes drift velocity to u and v in the scalar advection equations.

Wind stress in the model is applied to the upper boundary through the u and v component subgrid-scale mixing terms,

$$\frac{\partial}{\partial z}\left(\frac{\tau_x}{\rho} - K_m\frac{\partial u}{\partial z}\right), \quad (3a)$$

$$\frac{\partial}{\partial z}\left(\frac{\tau_y}{\rho} - K_m\frac{\partial v}{\partial z}\right) \quad (3b)$$

where τ_x is the zonal and τ_y is the meridional wind stress component, K_m is the eddy viscosity, and ρ is the surface water density. For simplicity, v_s and τ_y were set to zero in this study so that the wind and wave conditions always represented an east-west wind direction. With this simplification the Stokes drift was defined as

$$u_s = \left(\pi\frac{H}{\lambda}\right)^2\sqrt{\frac{g\lambda}{2\pi}}\exp\left[-4\pi\left(\frac{z}{\lambda}\right)\right] \quad (4)$$

where H is the wave height (twice the amplitude), λ is the wavelength, and g is the gravitational acceleration. This formula dictates that the effects of the vortex force terms described by (1) scale vertically to λ and are proportional to H^2.

The model was started from rest and forced using a spatially random surface heat flux perturbation to initiate circulations, as described by *Skyllingstad and Denbo* [1994]. In test cases with only wind or wave forcing, the random cooling was linearly reduced to zero during the first hour.

3. Results

Mixing processes in the ocean surface layer were examined in a series of experiments using idealized initial condition profiles taken from two regions of the Pacific Ocean (Figure 1). These profiles represent a relatively shallow (~45 m) mixed layer off of California and a relatively deep, winter mixed layer (~250 m) in the Gulf of Alaska (cases Mixed-Layer Dynamics Experiment (MILDEX) and C145, respectively). The temperature profile for the shallow mixed-layer case was taken from *Smith et al.* [1987] and represents typical conditions for the Pacific Ocean off the coast of California (Figure 1, left). Salinity was held constant in each of these experiments at 35.0 psu, and the latitude was set to 40°N. The model domain size was 320 by 320 m in the horizontal directions and 75 m in depth, with a grid spacing of 2.5 m and a time step of 5.0 s for the case MILDEX experiments. This domain size allows for five to six individual Langmuir cells with typical scales of 45 m. Initial conditions for the deep mixed layer experiments were prescribed using an idealized temperature profile based on measurements reported by *Pollard and Thomas* [1989] (Figure 1, right). Salinity was held constant at 34.5 psu, and a latitude of 46°N was used, corresponding to the observation site. The domain size was 1280 by 1280 m in the horizontal directions and 300 m in depth, with a grid spacing of 10 m and a time step of 16.0 s for case C145 experiments. As in case MILDEX, the domain size was selected so that five to six circulation cells could be simulated, assuming a cell size of ~200 m. Case MILDEX initialization was used for the majority of the experiments described here. Only the last experiment set uses case C145 initial conditions.

Three main experiment sets were performed. Initial growth of Langmuir circulations was examined in the first experiment and compared with observations and previous CL2 model results. We performed this comparison to see whether simulated Langmuir circulations grow at rates similar to observations and to determine whether model eddy viscosity controls growth of Langmuir circulations, as implied by theoretical results [*Leibovich*, 1983]. The second set of experiments also used the case MILDEX profile and concentrated on the response of the mixed layer to the type of surface forcing. In these experiments both the qualitative horizontal structure of the circulations and the mean profiles of temperature and velocity variances of the mixing processes were examined. We also calculated the resolved turbulent kinetic energy dissipation rates from the model and compared

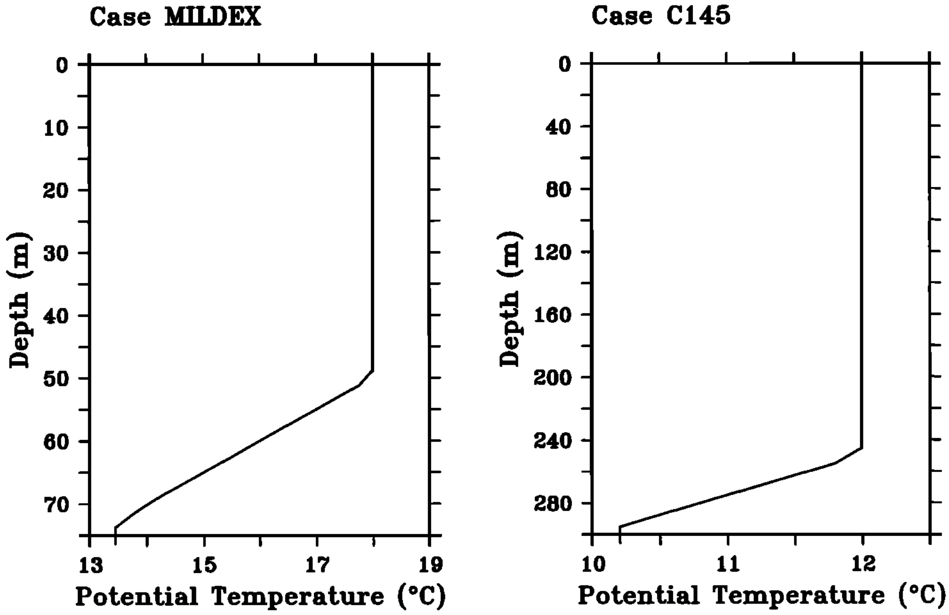

Figure 1. Idealized initial conditions of temperature representing the Mixed-Layer Dynamics Experiment (MILDEX) case [*Smith et al.,* 1987] and wintertime north Pacific, case C145 [*Pollard and Thomas,* 1989].

the results to observed dissipation rates. In the final set of experiments the response of a mixed layer to extreme forcing representing winter storm conditions was examined. These experiments were initialized using case C145 mixed-layer profile with surface wave and wind forcing representative of a moderate winter storm. Results from this simulation were compared with measurements of the temperature structure reported by *Pollard and Thomas* [1989].

3.1. Initial Langmuir Circulation Growth

Smith [1992] presents one of the few observations of Langmuir circulation growth. Smith demonstrated that the scale of Langmuir circulations can rapidly expand in response to increased surface wind forcing. This growth and scale transformation are examined in the first experiment, which exclusively considers forcing by the wind stress and the vortex force described by (1). The surface boundary conditions for this experiment were limited to wind stress τ = 0.15 N m^{-2} and vortex force term associated with waves of length λ = 40 m and height H = 1.5 m. These values represent typical conditions during MILDEX. To initiate motions in the model, cooling of -60 W m^{-2} was applied to the model surface at the beginning of the run and decreased to 0 in the first 15 min of the simulation. This small heat flux provided a finite random forcing that accelerates the initial Langmuir circulation growth.

Horizontal cross sections of the vertical velocity field and cross sections of the horizontal and vertical currents at the along-wind distance of 100 m are presented in Plates 1 and 2, respectively, showing the evolution of the Langmuir circulations. The initial circulation patterns have a consistent uniform appearance that is similar to the structure predicted by two-dimensional CL2 theory [e.g., *Li and Garrett,* 1993]. This pattern breaks down quite rapidly as the individual cells interact with one another between 36 and 52 min. By 60 min the Langmuir circulations form a complex system of connecting cells defining a crosswind scale of ~50 m and an along-wind scale of ~200 m. The vertical cross-section plot (Plate 2) shows that the breakdown of the strongly coherent cells between 36 and 52 min is accompanied by deepening of the circulations from 15 to ~30 m. The growth of the circulations after 44 min is consistent with observations presented by *Smith* [1992]. Smith found that the crosswind length scale of Langmuir circulations expanded rapidly over a 1-hour period in response to increased surface winds. Over the same time period, mixing from the circulations deepened from about 10 to 30 m, supporting the simulation results.

Leibovich and Paolucci [1981] used linear theory to show that the scale and growth rate for Langmuir circulations can be diagnosed using the Langmuir number, defined as

$$La = \left(\frac{K_m k}{u_*}\right)^{\frac{3}{2}}\left(\frac{S_o}{u_*}\right)^{-\frac{1}{2}} \tag{5}$$

where k=2π/λ is the surface wave wavenumber, K_m is the vertical eddy viscosity, S_o is the Stokes drift velocity defined as $S_o = 1/2\,(\pi H/\lambda)^2\,(g\lambda/2\pi)^{1/2}$, and u_* is the friction velocity defined as $u_* = (\tau_x/\rho)^{1/2}$. Using the prescribed wave conditions and a representative K_m from the subgrid-scale parameterization (K_m = 0.004 m^2 s^{-1}) yields an La of ~0.003. On the basis of linear stability diagrams calculated by *Leibovich and Paolucci* [1981], this value of La indicates that the scale of the most unstable Langmuir circulations is much smaller than the model grid spacing. However, the initial Langmuir circulation scale (~14 m) is of order five to six times the model grid spacing, which is roughly the smallest scale adequately resolved by the model. Therefore the initial Langmuir circulation scales are set by a numerical diffusion dependent on grid resolution and numerical smoothing. We can use the initial Langmuir cell size in conjunction with the Leibovich and Paolucci stability diagrams to estimate the value of an effective La and a corresponding numerical diffusion coefficient by inverting (5) and solving for K_m. This yields an effective La and K_m of ~0.02 and 0.015 m^2 s^{-1},

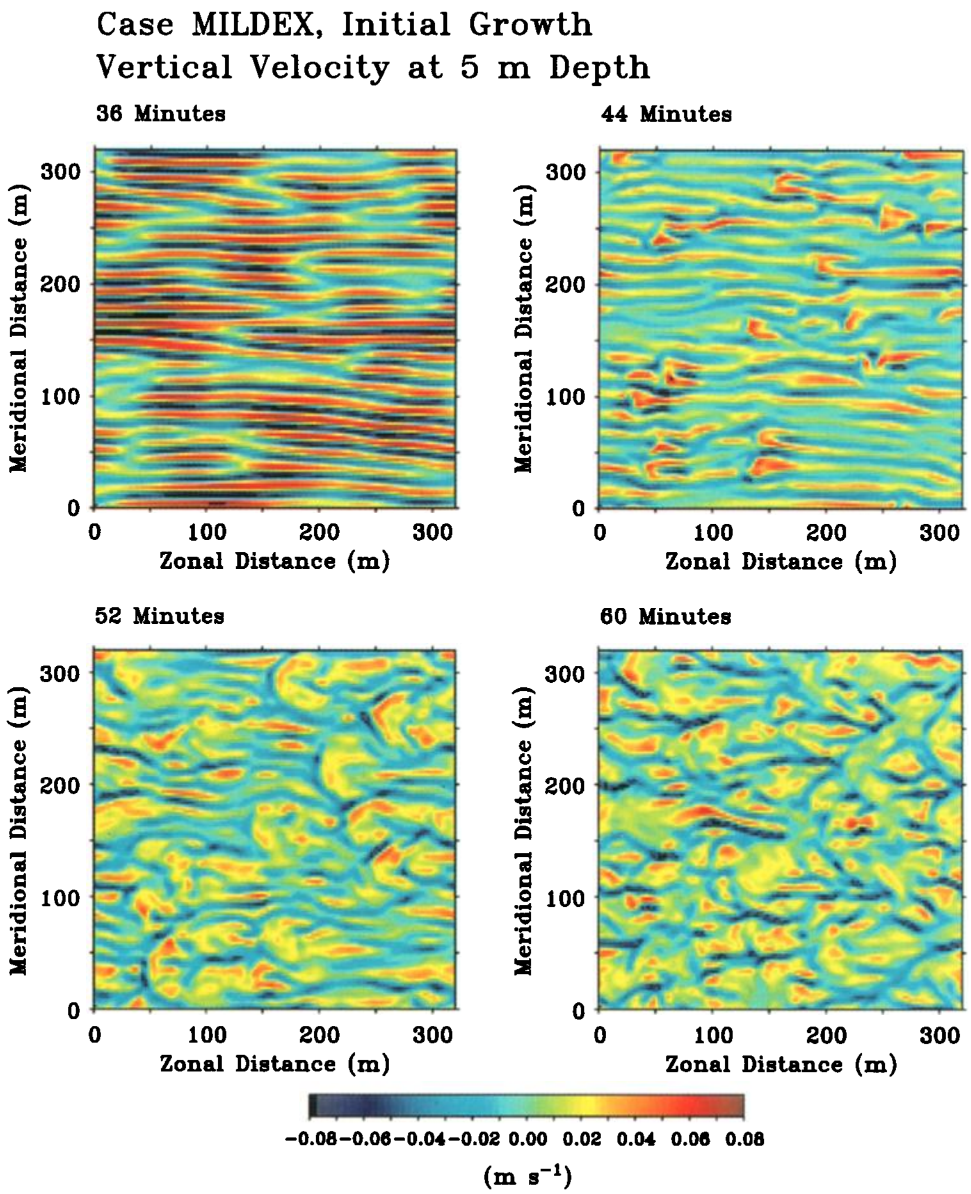

Plate 1. Plan view plots of the vertical velocity at 5 m depth as a function of zonal and meridional distance at 36, 44, 52, and 60 min. This plot shows the initial growth of resolution-dependent Langmuir circulations and their transition into mixed-layer-scale circulations. Initial condition for this case is from the MILDEX profile.

indicating that numerical diffusion is dominant in the initial growth of simulated Langmuir circulations. As shown later in this paper, fully developed Langmuir circulations are not governed as strongly by numerical diffusion and compare more favorably with observed scales for boundary layer turbulence and Langmuir circulations.

In calculating the effective *La* and K_m we are assuming that the linear analysis used by *Leibovich and Paolucci* [1981] is applicable to the current situation, even though diffusion by both resolved and numerical mixing is not taken into account. This points out a problem in applying linear theory for Langmuir circulations to an LES model with resolved turbulent motions. We cannot separate motions that are considered numerical diffusion and resolved turbulence (i.e., incoherent, isotropic) from those that are considered Langmuir circulations. Also, as pointed out by *Smith* [1992], analysis based on the CL2 equations that assume simplified shear and eddy viscosity profiles are not directly applicable to observed or modeled oceanic conditions. Both the shear and K_m vary significantly in the vertical and horizontal directions in our simulations, further demonstrating the difficulty in applying past CL2 model applications to the LES results.

3.2. Response Experiments: Qualitative Structure

In this section we examine the importance of wind, wave, and buoyancy forcing in determining the form and strength of vertical circulations in the surface mixed layer. A summary of the surface forcing for each of the response tests is outlined in Table 1. Each case is identified by a code representing the

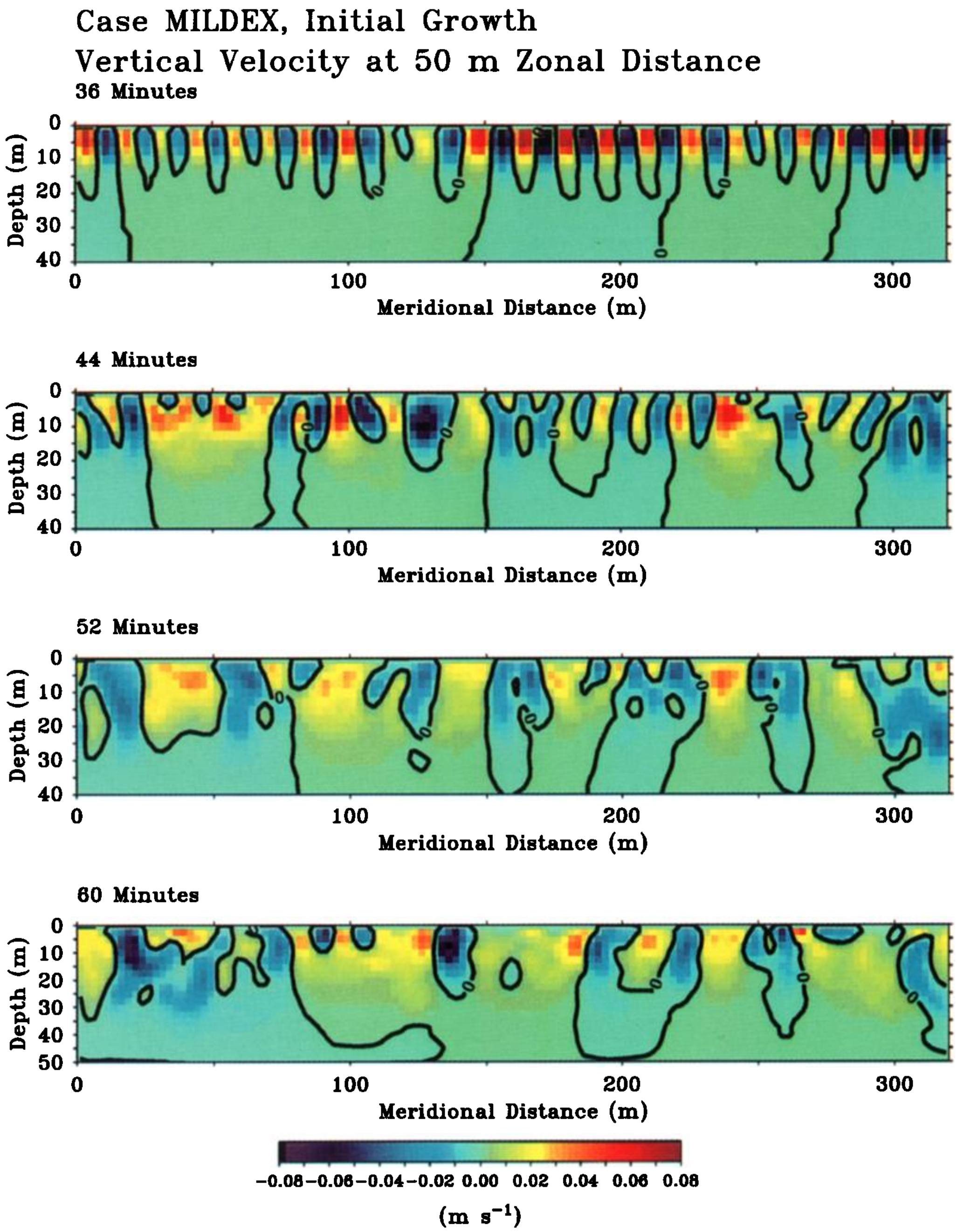

Plate 2. Cross sections of vertical velocity as a function of depth and meridional distance at zonal distance of 50 m. Plots are presented at 36, 44, 52, and 60 min, corresponding to Plate 1. These cross sections show the increase in depth and horizontal scale of the Langmuir circulations as the mixed layer becomes turbulent.

surface heat flux (C is cooling, H is heating), wind stress (W), and Stokes drift vortex force (S). Both cases HWS and HW are continuations of cases CWS and CW, in which surface heating represents a typical daily cycle (Figure 2). Cases HWS and HW represent the response of the mixed layer to daytime heating and stratification with and without the Stokes drift parameterization. Case MILDEX initial conditions and model domain parameters are used for these experiments.

Horizontal sections of vertical velocity at 5 m for the first four cases are shown in Plate 3, demonstrating the large influence that wind and wave forcing have on the mixed-layer circulation, in contrast to convection forced by surface cooling. For example, in case C a typical cellular pattern of convection is noted with broad regions of upwelling encompassed by narrow, linear downwelling zones, all having maximum velocities of ~0.02 m s^{-1}. The "spokelike" downwelling pattern evident in case C is consistent with similar downwelling structure reported in previous LES experiments, as noted by *Schmidt and Schumann* [1989]. This circulation pattern is quite different from case WS, where Langmuir circulations are forced that have strong, linear coherence aligned with the surface wind stress forcing.

Table 1. Response Experiments: Case MILDEX

Case	Heat W m^{-2}	τ_x, N m^{-2}	λ, m	H, m
C	-160	0.0	0.0	0.0
WS	0	0.15	40.0	1.5
CWS	-160	0.15	40.0	1.5
CW	-160	0.15	0.0	0.0
HWS	diurnal	0.15	40.0	1.5
HW	diurnal	0.15	0.0	0.0

Abbreviations are as follows: MILDEX, Mixed-Layer Dynamics Experiment; τ_x, zonal wind stress component; λ, wavelength; H, wave height; C, cooling; W, windstress; and S, Stokes vortex force.

Vertical velocities in these circulations range up to 0.06 m s^{-1}, with downwelling regions showing greater along-wind coherence than upwelling zones. The velocity amplitude, orientation to the right of the wind direction, and qualitative appearance of the simulated Langmuir circulations are in good agreement with measurements presented by *Smith* [1992] and *Thorpe* [1992]. In particular, the multiple scales of motion reported by *Thorpe* [1992] are evident in the simulation. A similar circulation pattern is noted in case CWS, which has surface cooling, wind stress, and the vortex force.

Given the relatively weak circulation generated by cooling alone (e.g., case C), it is understandable that case CWS is only slightly more vigorous than the case WS. The main effect of the surface cooling in case CWS is shorter downwelling segments and less alignment of the upwelling centers. When the vortex force is removed from the model (case CW), vertical circulations are of much smaller horizontal scale and have only weak coherence in the downwind direction. The vertical velocity field in case CW is only slightly stronger than in case C, indicating that shear instability near the surface does not significantly increase the strength of resolved turbulence above the level forced by buoyancy alone. The vortex force is also dominant when the model is forced with surface heating. Although surface heating leads to stratification of the simulated surface layer, both the vortex force (case HWS) and shear instability (case HW) are able to overcome the stabilizing effect of the stratification in the top 10 m. Again, the vortex force (case HWS) causes alignment of downwelling regions in the direction of the wind and wave forcing. Without the vortex force (case HW) the vertical velocity is considerably weaker in amplitude and does not show organized, aligned downwelling zones. Comparison of case HW to case CW shows circulations of similar amplitude in both examples, but the stabilizing effect of heating in case HW has led to a more distinct number of circulations with significantly larger scale in the horizontal direction (200 versus 20 m).

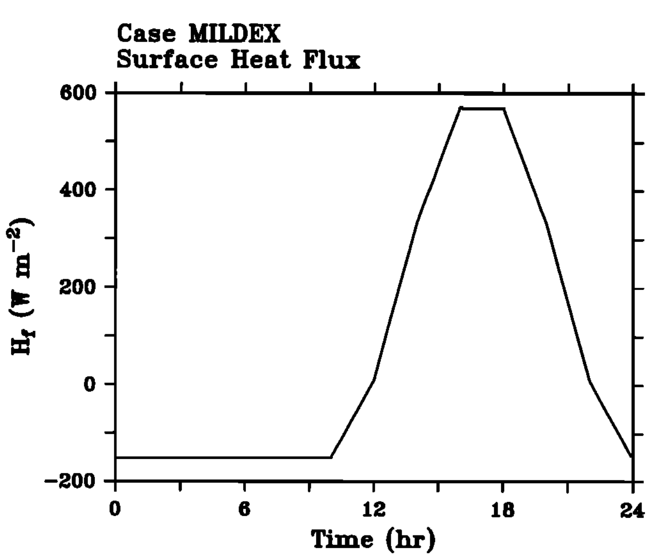

Figure 2. Daily cycle of the surface heat flux H_f for case MILDEX simulations.

The dominance of circulations driven by wave-current interaction (via the vortex force) over buoyancy-forced circulations is in general agreement with *Li and Garrett* [1995], who demonstrated a similar result using the CL2 model. They found that the importance of buoyancy forcing relative to surface wave forcing could be scaled using the Hoenikker number

$$H_o = \frac{\alpha g \dfrac{H_f}{(C_p \rho)}}{S_o k u_*^2} \qquad (6)$$

where α is the coefficient of thermal expansion (~1.5 x 10^{-4} K^{-1}) and C_p is the heat capacity of water at constant pressure (4000 J K^{-1}kg^{-1}). In our simulations, H_o varies between 0.058 during nighttime cooling to -0.188 during daytime heating. These values are well within the range where the vortex force is stronger than buoyancy forcing, as described by *Li and Garrett* [1995].

Overall, these results show that Langmuir circulations produced by the vortex force (cases WS, CWS, and HWS) are the dominant mixing process in the upper ocean mixed layer. This is particularly true for cases with surface heating (case HWS), where the Langmuir circulations are almost as strong at 5 m depth, as is the case with surface cooling (case CWS). Also, the simulations show that the form of circulations near the surface is highly dependent on the type of forcing, with the vortex force generating coherent structures that resemble Langmuir circulations.

The horizontal structure of the vertical velocity field at 20 m for the cases in Table 1 is presented in Plate 4. These plots are about midlevel in the mixed layer, which is below the depth of significant Stokes drift amplitude, as calculated with (4). At this depth, each of the cases has nearly equivalent vertical velocity amplitudes (0.04 m s^{-1}), with the exception of cases HWS and HW, which show weaker circulations (0.02 m s^{-1}) because of surface stratification. Significant alignment of the downwelling regions in cases CWS and WS is still evident, but with nearly equal length scales (~50 m) for both upwelling and downwelling areas and significantly larger horizontal separation between downwelling regions (100 versus 20 m). Comparison of case C with case WS shows that the vortex force creates circulations that are comparable in scale and strength to those produced by buoyancy forcing.

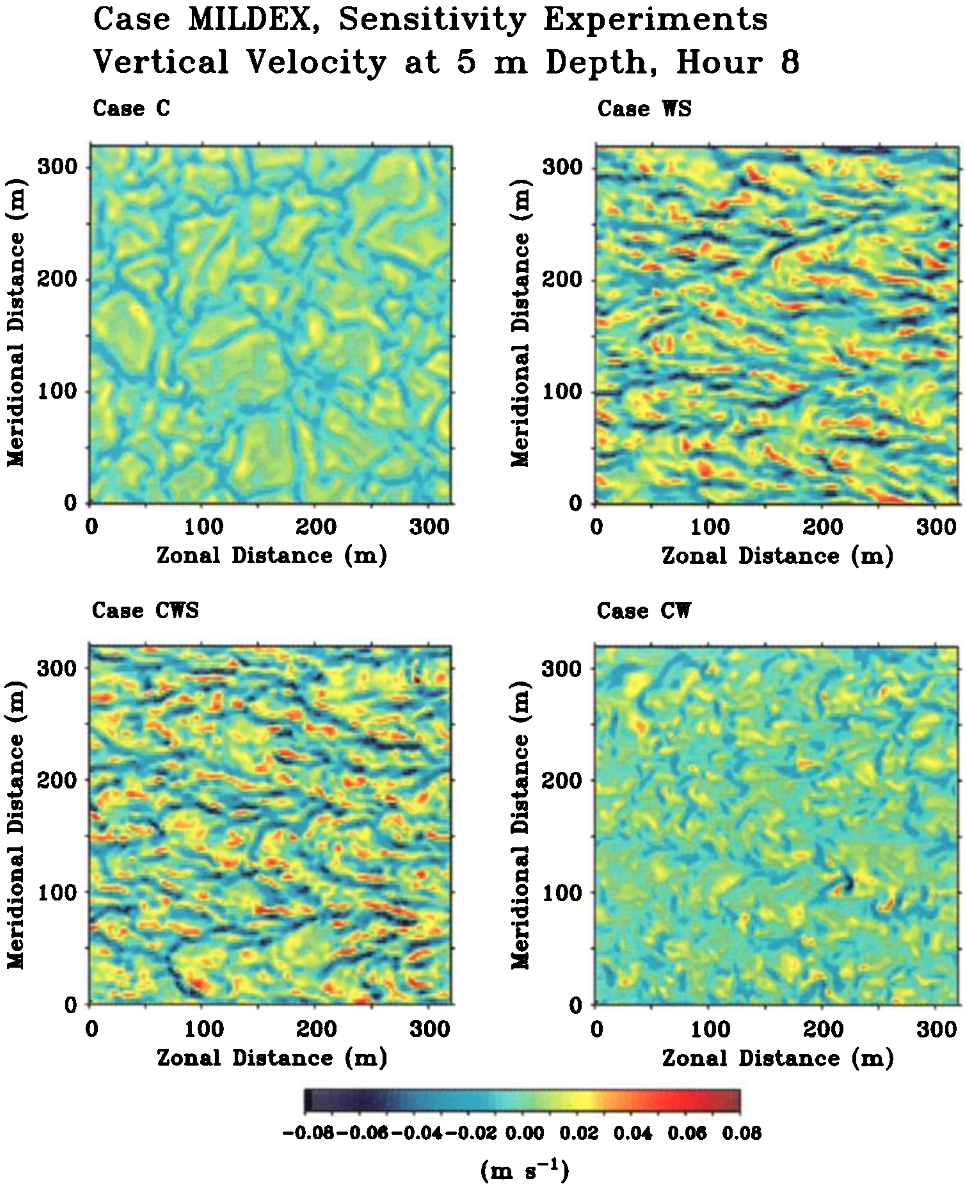

Plate 3. Plots of the vertical velocity at 5 m depth as a function of zonal and meridional distance for cases C, WS, CWS, CW, HWS, and HW, where C, H, W, and S, denote cooling, heating, wind stress, and Stokes vortex force, respectively (see Table 1). Cases C, WS, CWS, and CW are shown at hour 8, and cases HWS and HW are shown at hour 18.

The tendency for the vertical motion fields to have similar spatial characteristics away from the surface is also evident in a zonal cross-section plot of the vertical velocity (Plate 5). This plot shows how the vortex force parameterization forces strong, small-scale disturbances near the surface that are not transmitted to the middepth structure. Spectral analysis (presented later) shows an upward shift with depth in the peak velocity wavenumber confirming this behavior. The scale of circulations in each of the cases shown in Plate 5 changes as a function of depth so that eddies or coherent circulations approach a length scale that is proportional to the mixed-layer depth, as is characteristic for boundary layer flows [*Wyngaard*, 1992]. The exception to this rule might be case CWS, where the combination of cooling and the vortex force produce narrow downwelling regions that penetrate to ~30 m depth at ~110 and 270 m meridional distance. Plate 5 also shows the strong effect of the vortex force during daytime heating in case HWS. Circulations generated by the vortex force in this case maintain a 15-m mixed layer; in comparison, case HW has only weak vertical circulations near the surface.

Many of the features discussed by *Smith et al.* [1987] that identify Langmuir circulations are present in Plates 3 through 5. For example, the spacing of convergence zones that are roughly one to three times the mixed-layer depth is consistent with observations [*Leibovich*, 1983]. Probably the most noticeable feature of observed Langmuir circulations is the streakiness in surface debris or windrow patterns that appear on the ocean surface. We simulated this effect in the model by placing numerical "floats" at each grid point on the model surface for case CWS and case CW at hour 9 and moved the floats according to the instantaneous velocity field plus the Stokes drift velocity. The resulting float pattern is shown in Plate 6 at hour 10. For case CWS the simulated velocity field

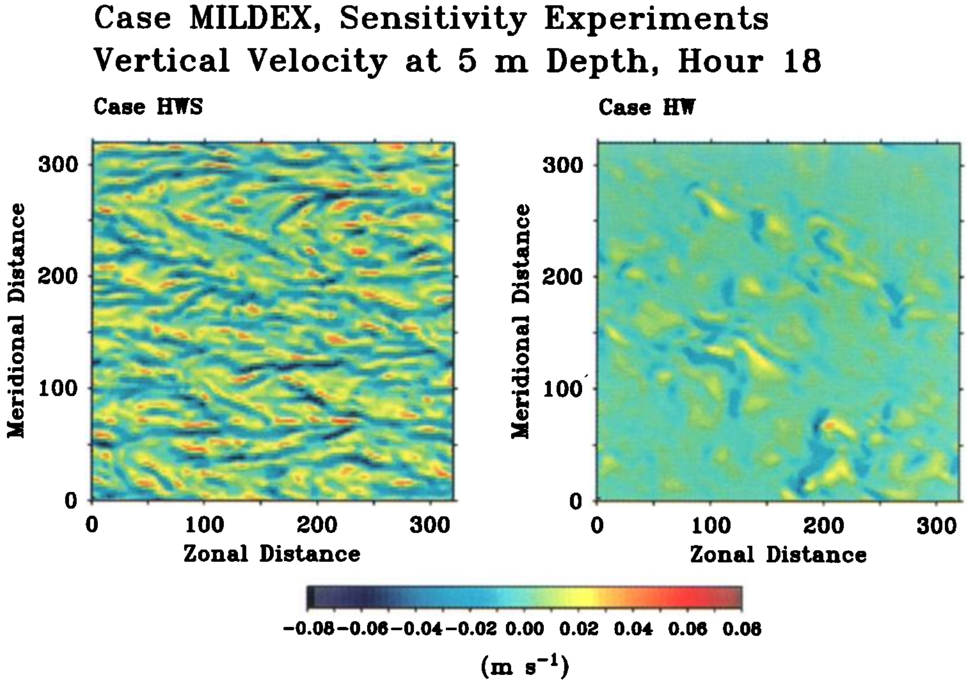

Plate 3. (continued)

has transported most of the surface floats into thin lines that correspond to the downwelling cells of the Langmuir circulations. This pattern is very similar to observations of bubbles by side-scan sonar [see *Thorpe,* 1992] and windrows that are commonly generated by waves on lakes and in the open ocean. In comparison, the float pattern for case CW is more random, with less zonal alignment.

Observations of bubble plumes using side-scan sonar show patterns that are similar to the float pattern presented in Plate 6. For example, *Farmer and Li* [1995] present results showing organized patterns in bubble distributions, with convergence lines forming Y junctions that typically point downwind. The simulated float positions also show convergence line junctions with predominantly downwind orientation, but with less organized structure than Farmer and Li's analysis. Differences between their observations and the model structures may be a result of the observed bubble plume analysis focusing on the strongest downward moving circulations, whereas the simulated float positions are more a function of the surface convergence pattern and may not represent the behavior of bubbles in suspension. Closer agreement between the modeled Langmuir circulations and Farmer and Li's results is apparent in the vertical velocity field for cases WS, CWS, and HWS shown in Plate 3. These plots show numerous Y junctions that consistently point downwind, corresponding to regions where bubble plumes would be transported downward.

The model also simulates the downwind "squirts" discussed by *Weller et al.* [1985] and *Smith et al.* [1987], but with lower absolute velocities (0.05 m s^{-1}) than observed (0.2 m s^{-1}), as shown in Plate 7. In these plots, the strongest regions of downward motion are accompanied by increased current velocities in the downwind direction. For example, in Plate 7 (top) at meridional distance of 40 m, downwelling of ~0.05 m s^{-1} is coincident with a 0.04 m s^{-1} downwind velocity peak. The lower velocities in the model result from a smaller wind stress value (0.15 N m^{-2}) than was measured by *Weller et al.* [1985] (0.35 N m^{-2}). Overall, the model produces circulations that are similar to measurements, although the heat flux, wind, and wave forcing conditions are not necessarily the same as those in the observed cases.

These results are supported by comparing scaled values of the maximum downwelling velocity, w_{down} and circulation pitch

$$Pt = \frac{u_{\text{conv}} - u_{\text{div}}}{w_{\text{down}}} \tag{7}$$

to the two-dimensional model results of *Li and Garrett* [1993]. Scaling for w_{down} and Pt is performed using

$$\frac{1}{u_*}\left(\frac{S_o}{u_*}\right)^{-\frac{1}{3}} \approx 50 \quad \text{, and} \quad \left(\frac{S_o}{u_*}\right)^{\frac{2}{3}} \approx 2.74 \;, \tag{8}$$

respectively. For case CWS, w_{down} is ~0.06 m s^{-1}, u_{conv} and u_{div} are ~0.06 m s^{-1} and -0.01 m s^{-1}, yielding a Pt of ~1.2. Scaling these values with (8) and applying results presented by *Li and Garrett* [1993] yields *La* of ~0.2 and 0.02 for Pt and w_{down}, respectively. Using these values of *La*, (5) can be inverted giving estimates for K_m of ~0.04 m s^{-2} for Pt and 0.01 m s^{-2} for w_{down}.

Both resolved and unresolved turbulence affects the strength of the Langmuir circulations in our simulations and the subsequent calculation of *La*. Determining a representative value of *La* requires an estimate of the effective eddy viscosity K_e, which accounts for mixing by resolved turbulence. An approximate K_e can be determined using

$$K_e = 0.1 l \bar{E} \tag{9}$$

where l is a turbulent length scale (~20 m for case CWS) and

$$\bar{E} = 1/2\left(\overline{u'^2} + \overline{v'^2} + \overline{w'^2}\right) \tag{10}$$

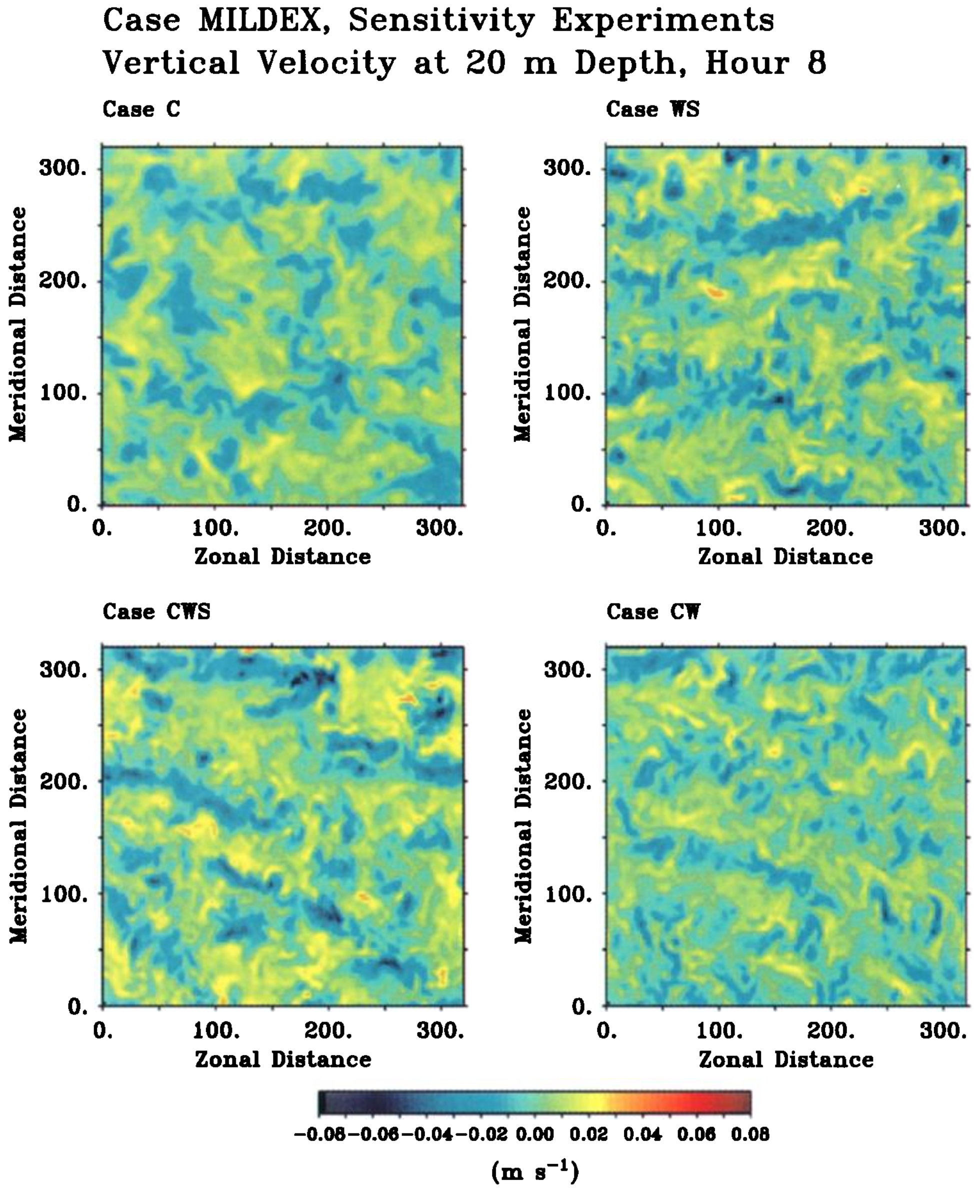

Plate 4. Same as Plate 3, but located at 20 m depth.

is the horizontally averaged resolved turbulent kinetic energy [*Deardorff,* 1980]. The resolved turbulent velocity components are calculated by removing the horizontally averaged momentum from the momentum fields,

$$\varphi' = \varphi - \sum_x \sum_y \varphi \tag{11}$$

where φ is u, v, or w and summation symbols represent a horizontal average. Combining (9) and (5) yields profiles of K_e and La as shown in Figure 3 that are between values diagnosed with w_{down} and Pt shown above or in general agreement with *Li and Garrett*'s [1993] results. Li and Garrett note that the two-dimensional model consistently under predicts the strength of pitch Pt in comparison to observations. The LES model Pt is in better agreement with observations, however, the choice of l and variation of K_e leaves too much variability to conclude that the LES model results are significantly different from the two-dimensional Li and Garrett solutions.

3.3. Response Experiments: Mean Profiles

Qualitative analysis of the near-surface vertical motion field indicates consistent differences between cases with and without the vortex force. To more clearly distinguish the effects of the surface heat flux, wind stress, and vortex force parameterization, we follow quantitative analysis techniques used in atmospheric mixed-layer studies as described by *Wyngaard* [1992]. Typically, these techniques attempt to compare measurements and model results by scaling horizontally averaged quantities, such as the average vertical velocity variance or average vertical heat flux, with surface forcing parameters. The main assumption is that turbulent boundary layers behave in a similar manner that is independent of the scale of the system. This assumption may not be as applicable in the present analysis, because observed velocity data for ocean or lake surface layer turbulence are not available for comparison. As proxy data, we compare the simulated mean fields with atmospheric and laboratory tank

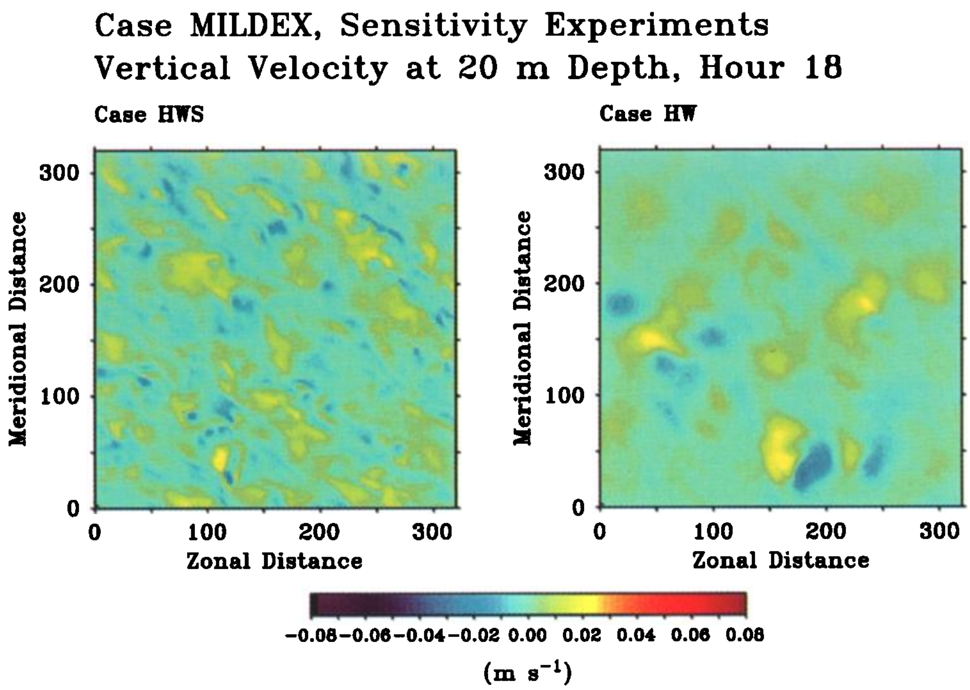

Plate 4. (continued)

data, which do not have the effects of wave-current interactions but can show the relative influence of wind and wave effects. Scaling parameters of vertical velocity, horizontal velocity, and temperature used for this comparison are defined as

$$w_* = (\beta g z_i H_f)^{1/3}, \tag{12a}$$

$$u_* = \sqrt{\frac{\tau_x}{\rho_o}}, \tag{12b}$$

$$T_* = \frac{H_f}{w_*}, \tag{12c}$$

where β is the volumetric expansion coefficient for seawater, g is the gravitational acceleration, z_i is the mixed-layer depth, and H_f is the surface heat flux [*Deardorff*, 1972].

Plots of the scaled, horizontally averaged resolved variances of vertical velocity $<w'^2>$, horizontal speed $<V'^2>$ where

$$V' = (u^2 + v^2)^{1/2} - \langle (u^2 + v^2)^{1/2} \rangle, \tag{13}$$

and the heat flux, $<w'\Theta'>$, are shown in Figure 4 for cases C, CW, CWS, and WS. The average variance profiles represent the kinetic energy contained in the resolved eddy motions and indicate the strength of mixing as a function of depth. The subgrid-scale fluxes, which can have a significant effect near the surface, are not included in these profiles. For example, $<w'\Theta'>$ decreases at the surface, where the simulated heat flux is entirely defined by the subgrid-scale model. Figure 4 also shows scaled data from laboratory measurements taken by *Willis and Deardorff* [1974] and *Deardorff and Willis* [1985], and aircraft data from *Lenschow et al.* [1980]. These data represent a convective boundary layer without surface wind stress effects, corresponding to case c. Accordingly, $<w'^2>$ from case C is in good agreement with these measurements. The location of the maximum $<w'^2>$ at the center of the mixed layer for case C is consistent with symmetric eddies that are confined between the ocean surface and the thermocline. With wind stress forcing (case CW) the magnitude of $<w'^2>$ increases and the peak value is shifted slightly toward the surface. In this case, the addition of momentum from the wind stress forces stronger turbulent eddies that are influenced by shear instability near the surface.

The two cases with the vortex force parameterization, cases WS and CWS, demonstrate the dramatic effect (see Plate 3) of Langmuir circulations on the strength of the near-surface eddies. For case WS, $<w'^2>$ is a maximum just below the surface and decreases rapidly with depth. A similar profile shape is obtained in case CWS, but with higher $<w'^2>$ throughout the mixed-layer depth because of the combined surface forcing. Interestingly, the CWS profile matches case CW below about $z/z_i = 0.75$, suggesting that the strength of circulations near the bottom of the mixed layer is primarily a function of the combined buoyancy and shear forcing, and not of the vortex force. The vortex force at this depth is minimal because of the exponential decay with depth of the Stokes drift given by (4). For scaled $<V'^2>$ an obvious difference exists between case C and the cases with applied wind stress. With wind stress the profile of $<V'^2>$ is a maximum at the surface and decreases rapidly to a near steady value below $z/z_i = 0.2$. For case C the variance is much smaller throughout the mixed layer, with maxima at the top and bottom of the profile where the largest eddies have the strongest horizontal divergence. For cases CWS and WS, $<V'^2>$ at the surface is nearly two times greater than $<V'^2>$ for case CW, showing the effect of the vortex force on the surface current variability. The larger $<V'^2>$ in the cases with the vortex force results from the downwind jets that appear in regions of convergence in the Langmuir circulation cells, as shown earlier in Plate 7.

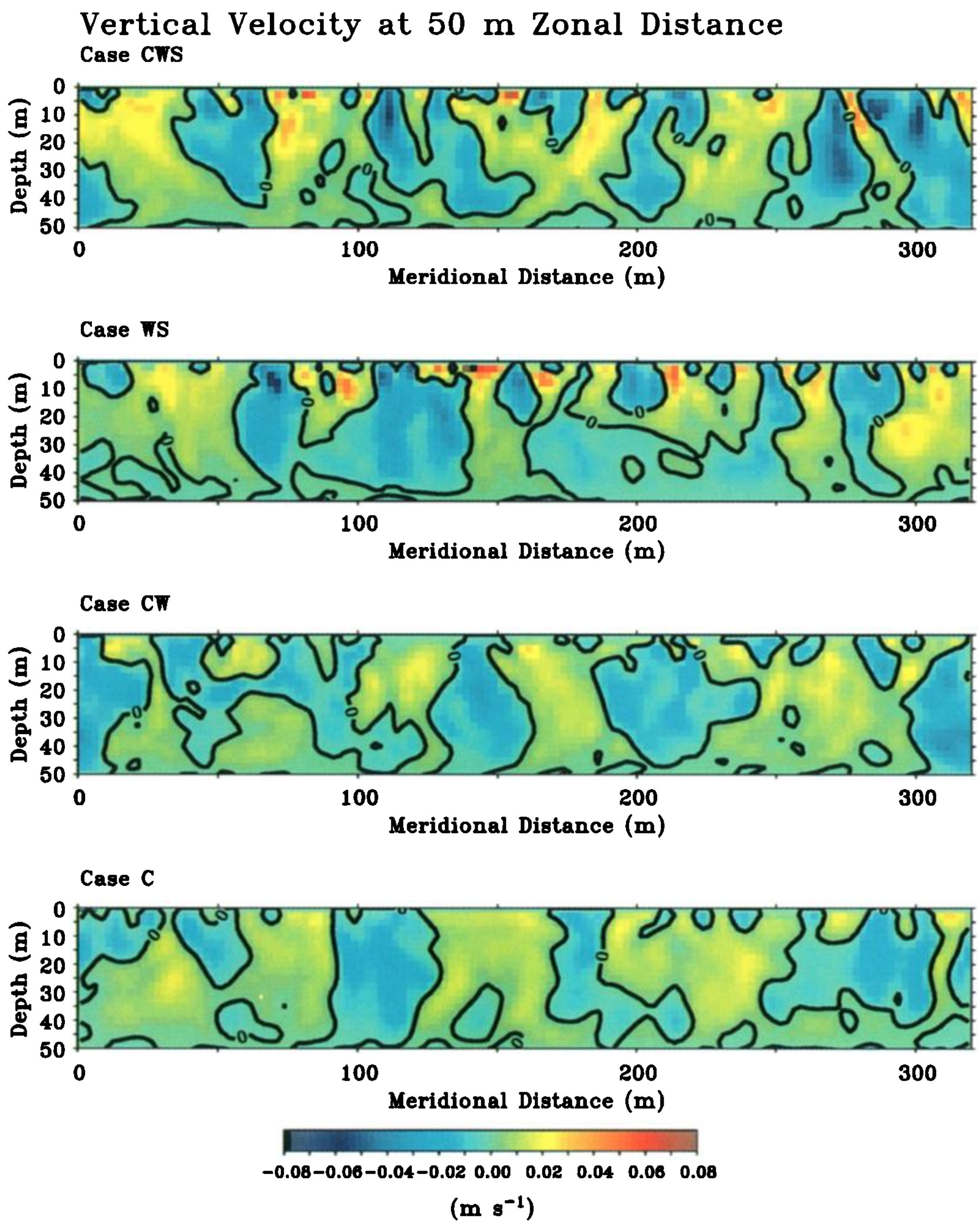

Plate 5. Cross sections of vertical velocity as a function of depth and meridional distance at zonal distance 50 m. Plots are presented for case CWS, WS, CW, and C at hour 8 and HW and HWS at hour 18.

Simplified models of the mixed layer, such as the *Mellor and Yamada* [1982] turbulence closure or the *Garwood* [1977] bulk-layer model, use estimates of the mixed-layer turbulence kinetic energy to determine vertical mixing and the growth of the mixed layer. The profiles of $<w'^2>$ and $<V'^2>$ produced by the simulations show that wave-current interaction may be an important source of turbulence that is currently not included in vertical mixing parameterizations. Turbulence produced by surface wave effects could be significant, particularly during strong storm events that may be responsible for the majority of the seasonal mixed-layer growth at high latitudes [*Large et al.*, 1986].

Also shown in Figure 4 is the scaled heat flux profile, $<w'\Theta'>$, which displays a consistent pattern for the cases that have surface cooling. For these cases, $<w'\Theta'>$ is a maximum at the surface and decreases to negative values at the base of the mixed layer. As expected, case WS does not show a significant heat flux, except at the bottom of the mixed layer, where relatively colder water is being entrained upward by mixed-layer eddies leading to a negative heat flux. The strength of entrainment mixing is about the same for each case, with the exception of case CWS, which has a $<w'\Theta'>$ about a factor of 2 greater than that shown in the other experiments. The increase in entrainment with case CWS results from the significant higher turbulent energy, $<w'^2>$ and $<V'^2>$, as shown in Figure 4. A plot of $<w'\Theta'>$ at the top of the thermocline (Plate 8) shows significantly more activity for case CWS when compared with the other test cases. The entrainment is produced by plumelike features that transport relatively warm water downward in limited regions. Cross-

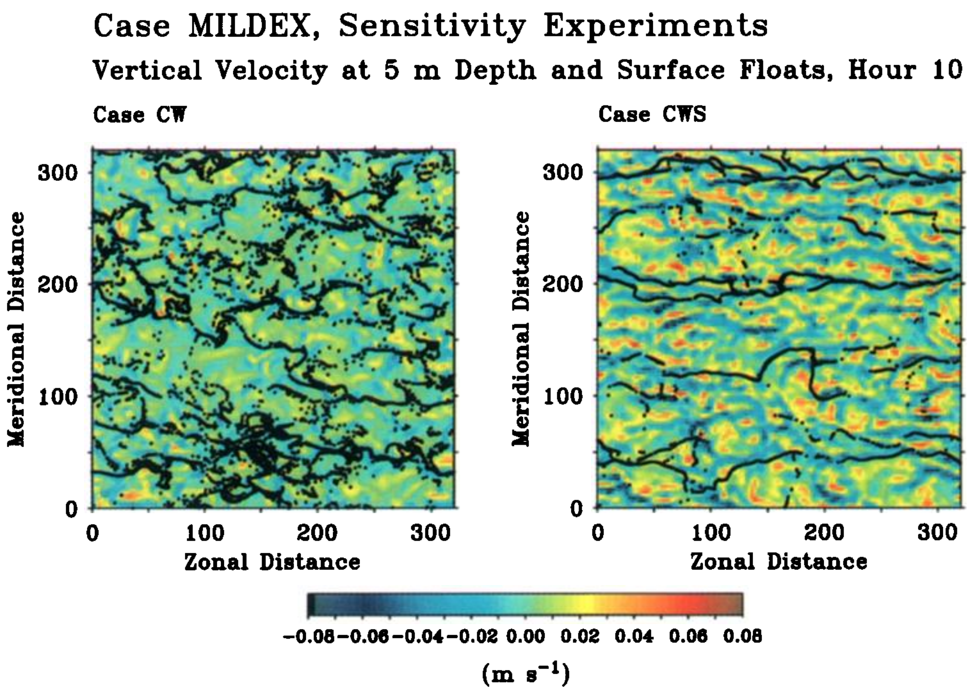

Plate 6. Plots of the vertical velocity at 5 m depth and location of surface floats after 1 hour of transport by the surface currents and the Stokes drift for cases CW and CWS. Both plots are at hour 10 in the simulations.

section plots (i.e., Plate 5) show that these plumes extend downward from the central portion of the mixed layer and are extensions of the largest-scale eddies. The model results do not show significant entrainment mixing from shear instability at the bottom of the mixed layer, but indicate that overshooting plumes cause the majority of the mixed-layer growth.

The large increase in the heat flux for case CWS is significant, because it indicates that wave-current interactions can enhance entrainment during mixed-layer deepening and,

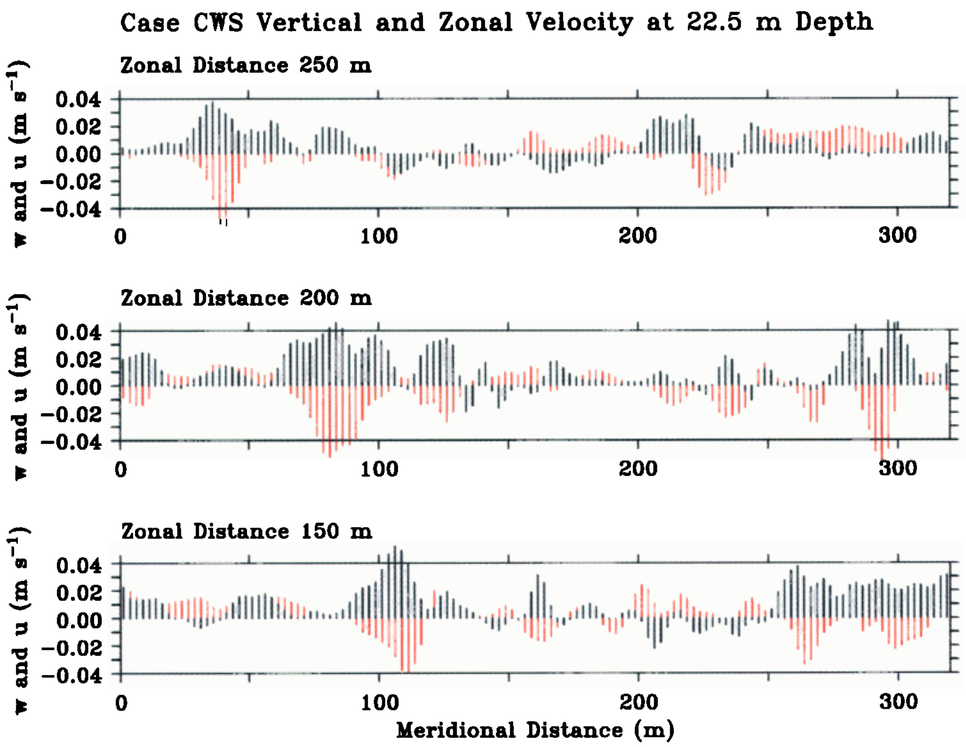

Plate 7. Stick plots of the vertical velocity (red) and horizontal velocity (blue) at 22.5 m depth corresponding to similar observations of velocity reported by *Weller et al.* [1985]. Plots are presented at zonal distance 150, 200, and 250 m as a function of the meridional distance..

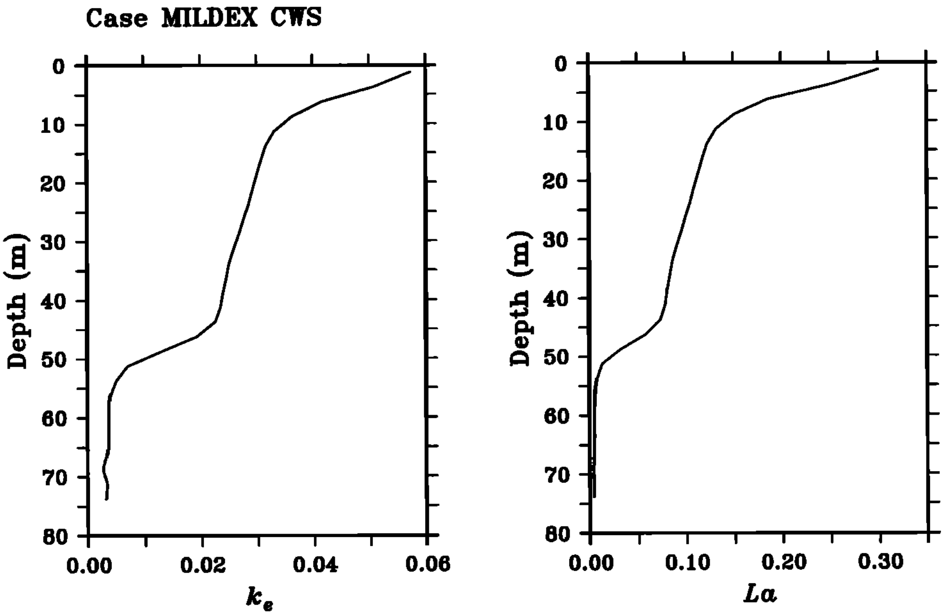

Figure 3. Plots of the effective eddy viscosity K_e and corresponding Langmuir number La for case CWS at hour 8. These values are estimated using the resolved turbulent kinetic energy.

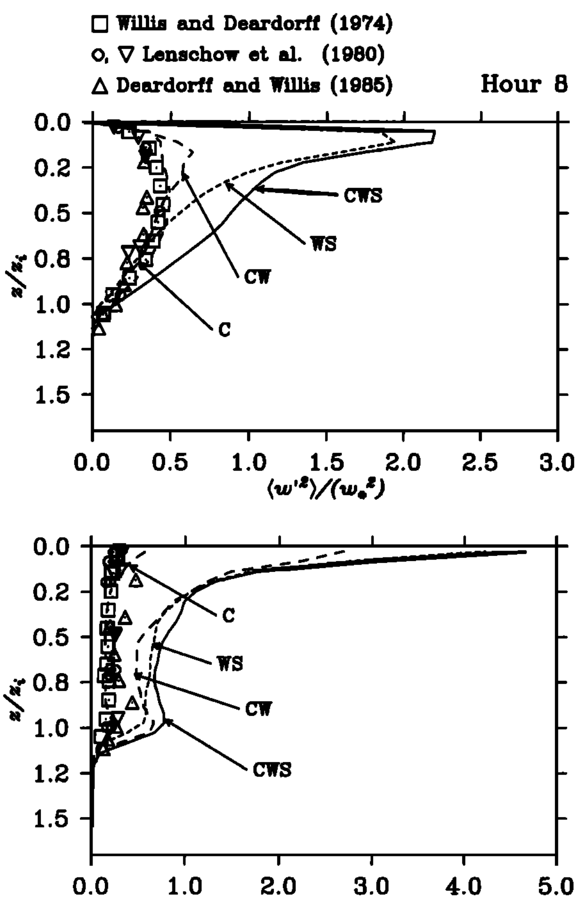

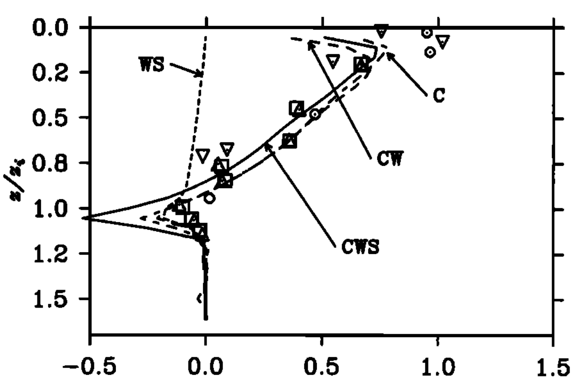

Figure 4. (continued)

Figure 4. Plots of the scaled average variance of vertical velocity $<w'>$, horizontal speed $<V'>$, and heat flux $<w'\Theta'>$ at hour 8 as a function of depth scaled by mixed-layer depth z_i. Also shown are laboratory data from *Willis and Deardorff* [1974] and *Deardorff and Willis* [1985] and atmospheric data from *Lenschow et al.* [1980].

ultimately, affect sea surface temperature. In most bulk layer, one-dimensional models of the mixed layer, entrainment rate estimates are based on a budget of turbulence kinetic energy generated by wind-forced shear instability and buoyant forcing. The simulations presented here show that wave-current interactions should not be overlooked in estimating the strength of mixed-layer entrainment and should be included in one-dimensional models of the ocean surface mixed layer.

3.4. Response Experiments: Turbulent Dissipation Rates

Shay and Gregg [1986] and *Lombardo and Gregg* [1989] showed that the ocean surface mixed layer can be characterized using a similarity approach developed in atmospheric boundary layer research. In general, turbulence data in the ocean mixed layer are limited to measurements of the turbulence kinetic energy dissipation rate ε, which has characteristic scales that depend on the relative influence of surface heating and wind stress forcing. For cases with strong surface cooling, ε scales according to

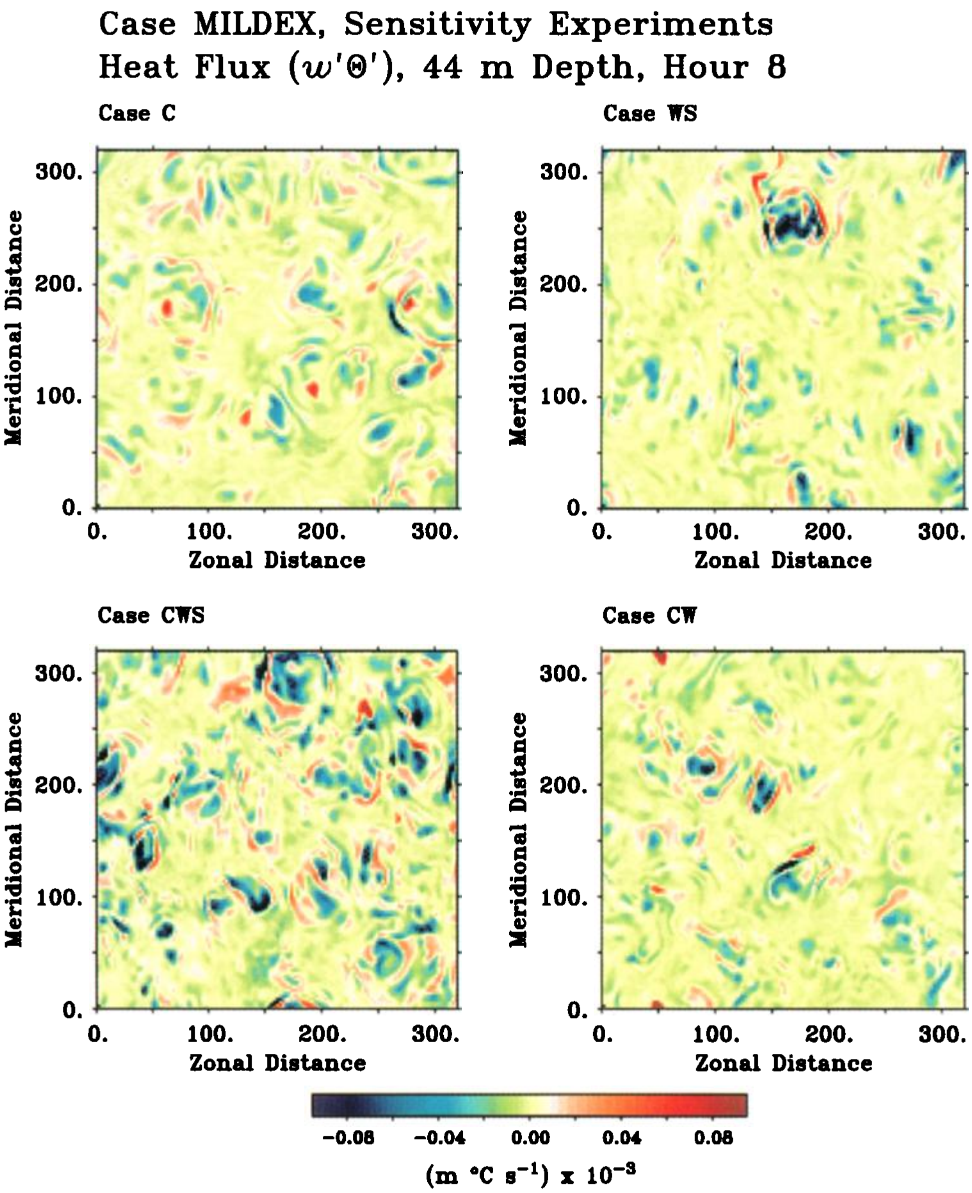

Plate 8. Plots of the vertical heat flux $w'\Theta'$ at 44 m depth as a function of zonal and meridional distance for cases C, WS, CWS, CW, where C, W, and S, denote cooling, wind stress, and Stokes vortex force, respectively (see Table 1).

$$\varepsilon_{ml} = J_b^o \tag{14}$$

where $J_b{}^o$ is the surface buoyancy flux defined as

$$J_b^o = -\frac{g\alpha}{\rho C_p} J_q^o , \tag{15}$$

α is the coefficient of thermal expansion (-2.5 x 10^{-4} K^{-1} at 20°C), C_p is the specific heat of seawater at constant pressure, and $J_q{}^o$ is the surface heat flux. When wind stress dominates, ε scales as

$$\varepsilon_s = \frac{u_*^3}{\kappa z} \tag{16}$$

where u_* is the friction velocity defined as $u_* = (\tau/\rho)^{1/2}$ and κ is von Karman's constant ($\kappa = 0.4$).

To compare the model with theory and observations, we computed ε from the resolved model velocity field by assuming that the simulated vertical velocity field follows the shape of the theoretical Kolmogorov spectrum,

$$\Phi_w(k) = \frac{4}{3}\alpha_1 \langle\varepsilon\rangle^{2/3} k^{-5/3} \tag{17}$$

where k is the horizontal wavenumber and $\alpha_1 \sim 0.52$. Making this assumption is acceptable as long as the turbulent motions are isotropic and are inertial (i.e., are not dominated by strong body forces). A plot of the wavenumber spectra of w for cases C and CWS is presented in Figure 5, along with scaled laboratory measurements of *Deardorff and Willis* [1985]. This plot shows that the spectral density of the simulated turbulent eddies is in agreement with the laboratory data for case C, but is stronger in amplitude for case CWS near the surface, where

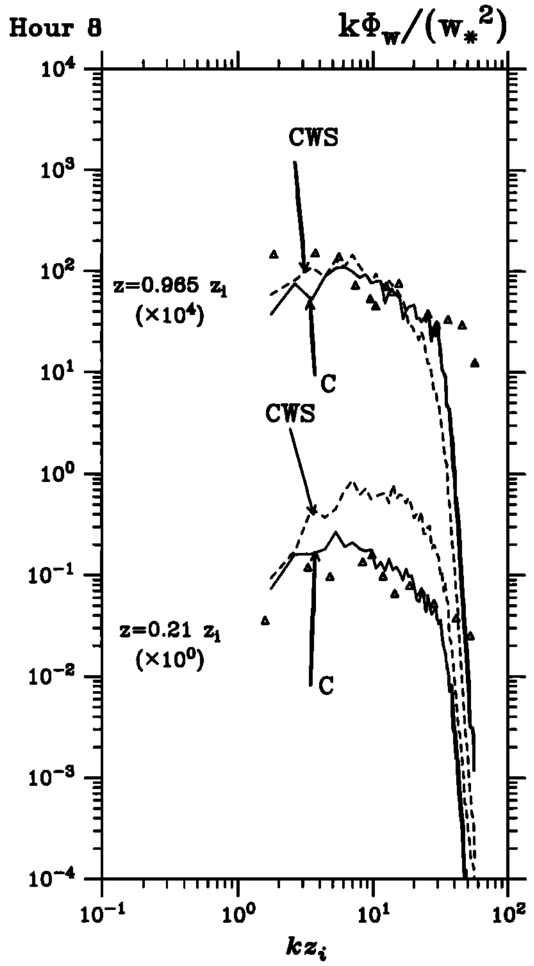

Figure 5. Scaled horizontal wavenumber spectra of the vertical velocity Φ_w for cases CWS and C at hour 8 as a function of the wavenumber k scaled by the mixed-layer depth z_i. Also shown are spectra measured from a laboratory tank experiment (taken from *Deardorff and Willis* [1985]). The spectra are from depths of 0.21 and 0.965 of the mixed-layer depth.

Langmuir circulations are dominant. The spectral curves follow the $k^{-5/3}$ form predicted by (17) over a range of wavenumbers until subgrid-scale processes become important. Differences in the two spectral curves are noted near the surface, where the Stokes drift parameterization forces smaller-scale motions and a shift in the spectral peak. Dissipation rates were estimated from (17) by computing the average horizontal spectra $\Phi(k)$ over $kz_i = 6$ to 20 at each level and solving

$$\langle \varepsilon \rangle = \left\langle \left[\frac{3}{4\alpha_1} \frac{\Phi_w(k)}{k^{-5/3}} \right]^{\frac{3}{2}} \right\rangle \tag{18}$$

A plot of the scaled ε for cases C, CWS, and CW is shown in Figure 6, along with representative measurements from *Lombardo and Gregg* [1989]. Both the along-wind (zonal) and crosswind (meridional) calculated ε are plotted in Figure 6, showing the anisotropic effect of simulated Langmuir circulations on the dissipation rates near the surface (case CWS). For case C, the scaled model ε profile agrees closely with the shape and strength of observed dissipation rates. Cases C and CW also show that, without the vortex force, ε does vary significantly between the zonal and meridional directions. Compared with case C, ε profiles for cases CWS and CW do not agree as well with observations, but the modeled ε is still within the measurement error for case CWS. The shape of the modeled ε profile below 10 m fits a $1/z$ function, as predicted by (9), indicating similarity between the model turbulence and observations. It is not surprising that the model underestimates the strength of eddy motions for the wind-driven case, because the original subgrid-scale turbulence parameterization used in the model was designed for simulating strongly convective flows and is not calibrated accurately for sheared flows. Also, the precise value of the dissipation rate for cases with the vortex force is somewhat questionable because of the anisotropic behavior of the velocity field. Nonetheless, the modeled ε does show the effect of Langmuir circulations above 10 m for case CWS,

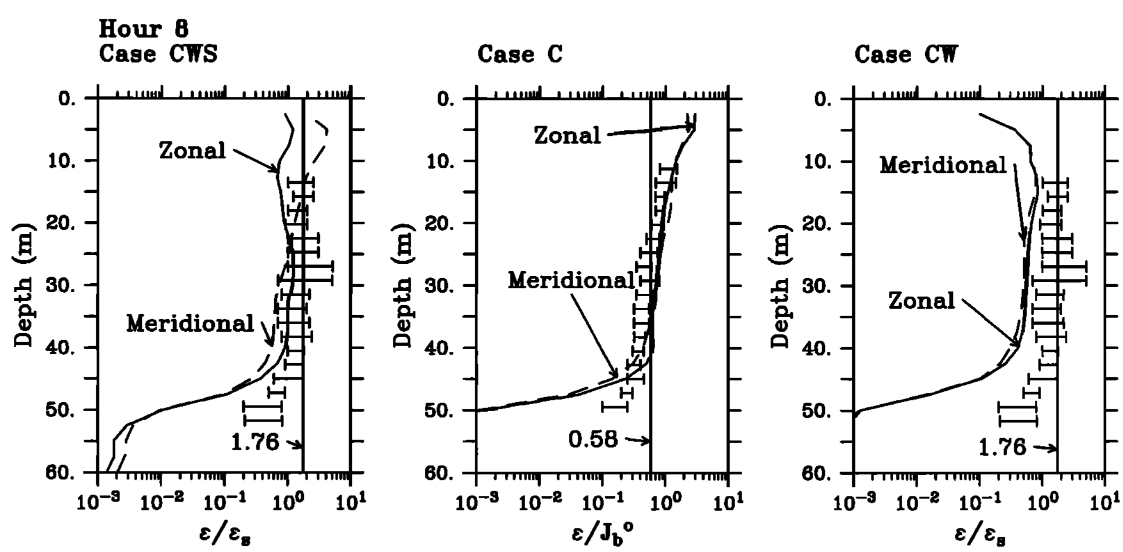

Figure 6. Plots of the modeled and observed scaled turbulence dissipation rate ε calculated using zonal and meridional Fourier transforms of the vertical velocity w as a function of depth at hour 8 for cases C, CW, and CWS. Scaling for ε is the surface buoyancy flux for case C and ε_s for cases CWS and CW (see text for description). The observations are taken from *Lombardo and Gregg* [1989] and represent the significance ranges for their dissipation rate calculations.

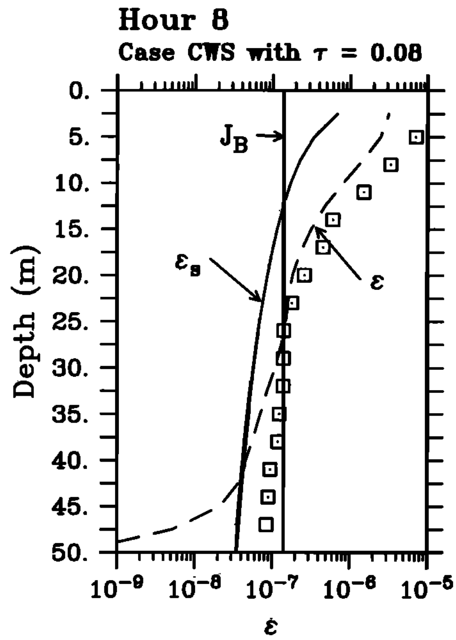

Figure 7. Turbulence dissipation rate ε calculated using the meridional Fourier transform for case CWS with $\tau = 0.08$ as a function of depth at hour 8. Also shown are the buoyancy flux J_B, similarity dissipation rate ε_s, and observed ε from *Anis and Moum* [1992].

particularly for the crosswind transform case, where ε exceeds the theoretical value. In general, these results illustrate that the model produces turbulent motions that are statistically similar to observed motions. In cases with Langmuir circulations the simulations show that the scaled ε does not significantly exceed similarity values, except near the surface where ocean measurements are not readily available.

Anis and Moum [1992] present measurements of the near-surface ε that exceed the similarity scaling of both (14) and (16), indicating that wave effects might cause an increase in the surface turbulence. Wind stress was moderate during their measurements (0.08 N m^{-2}), significant wave heights were 0.5 m for wind waves and 2.0 m for swell, and the surface cooling varied between 166 and 212 W m^{-2}. To assess the importance of wave forcing with reduced wind stress, we performed a simulation using the wave conditions of case CWS, but with wind stress reduced to 0.08 N m^{-2} and the cooling rate increased to -200 W m^{-2}. A plot of ε from this simulation is shown in Figure 7, along with measured ε taken from Anis and Moum (Figure 7, squares). This plot shows that the simulated ε is greater than J_b^o and ε_s over the entire profile, supporting the interpretation given by Anis and Moum that ε in the upper 20 m is enhanced by a combination of Langmuir circulations and increased turbulence from the wave-drift currents. Moreover, the simulation demonstrates that wave-current interactions may dominate the surface-layer turbulence, even when the wind stress is relatively weak.

Increased turbulence dissipation in the simulations, above similarity theory values, may be a result of surface wave energy being transferred to Langmuir circulations without a corresponding decrease in the surface wave intensity. Because surface waves are forced by the wind stress, maintaining the surface wave field at a constant height as is done in the simulations is an added source of energy and could be equivalent to applying a larger wind stress. The contribution of the vortex force terms to the horizontally averaged total kinetic energy can be expressed as (see appendix for derivation)

$$\overline{\frac{1}{2}\frac{\partial v^2}{\partial t}} = u_s \overline{u'\frac{\partial w'}{\partial z}} \tag{19}$$

$$\overline{\frac{1}{2}\frac{\partial w^2}{\partial t}} = u_s \overline{\frac{\partial u'w'}{\partial z}} - u_s \overline{u'\frac{\partial w'}{\partial z}}, \tag{20}$$

where we have assumed only a zonal Stokes drift. Equations (19) and (20) show that the Stokes drift affects the kinetic energy for the vertical and crosswind velocity and does not directly increase or reduce the average kinetic energy in the same direction as the wind stress. Langmuir circulation kinetic energy depends on the interaction between the surface wind stress and the Stokes drift as shown by combining (19) and (20) and vertically integrating,

$$\frac{1}{2}\frac{\partial(v^2 + w^2)}{\partial t} = u_s(\overline{u'w'})_{\text{top}} = u_s u_*^2. \tag{21}$$

Equation (21) demonstrates that increased kinetic energy from surface waves is dependent on both the wind stress and Stokes drift or wave properties. Interestingly, (21) shows that similar kinetic energy changes can be produced by high wind stress, low-amplitude wave cases, as with low wind stress, high-amplitude wave cases. However, the vertical distribution of energy in these two situations would be different, as shown by (19) and (20).

A more complete energy budget for surface waves and associated turbulence is needed to resolve the issue of how wind energy is transferred to Langmuir circulations and mixed-layer turbulence. Nevertheless, observations tend to show consistently larger dissipation rates than can be explained by similarity scaling or wind stress acting alone, suggesting that surface waves are important in forcing increased turbulent energy.

3.5. Strong Wind Case: North Pacific Wintertime

Wind forced mixing is known to have a significant role in determining the seasonal cycle of the mixed-layer depth throughout the world ocean. However, very few observations exist that document the importance of Langmuir circulations in controlling the temperature structure and depth of the wintertime mixed layer. Using data from a drifting spar buoy, *Pollard and Thomas* [1989] presented evidence that Langmuir circulations may have a large influence on the mixed-layer temperature structure during daytime heating in late winter (March). Their measurements showed that the temperature as deep as 145 m was increasing during the daytime heating period, when convective mixing was suppressed. From these data they calculated a vertical heat flux during a 6-day study period that could not be reconciled with the known surface heat budget. In a companion paper, *Thomas* [1989] used a simple circulation model and concluded that the spar buoy was advected into the convergent downwelling region of a Langmuir circulation. Temperatures measured by the buoy in the convergent zone were biased toward recently transported surface water conditions and therefore gave erroneous heat flux values.

Table 2. Strong Wind Case: North Pacific Wintertime, Case C145

Case	τ_x, N m^{-2}	λ, m	*H*, m
C145-W	0.35	0.0	0.0
C145-WS	0.35	100.0	5.0

See Table 1 for definitions.

We performed two modeling experiments (Table 2) to determine whether Langmuir circulations could cause a localized increase in temperature in the middle of the mixed layer during daytime heating, as hypothesized by *Thomas* [1989]. The initial temperature profile for these experiments is shown in Figure 1, labeled case C145. For these cases, the model was run for 1.5 daily cycles (Figure 8), and analysis was performed from hour 12 to hour 36.

Horizontal cross sections of the temperature and vertical velocity at 45 and 125 m from the two experiments illustrate how the Langmuir circulations modify the temperature structure during daytime heating (Plate 9). At 45 m, case C145-WS shows linear downwelling regions, where the temperature is up to 0.03°C warmer than the surrounding upwelling regions. In comparison, case C145-W has a temperature difference greater than 0.04°C over most of the domain, but without directional dependence. Also, the vertical motion field for this case has less amplitude. The two cases have more pronounced differences at 125 m depth, where case C145-W has small horizontal temperature variation in contrast to C145-WS. Downwind coherence is not apparent for either case at 125 m, but significant vertical velocities are evident with case C145-WS that are coincident with local regions of warm water. These results also point out the importance of the horizontal wavelength of the surface waves in setting the depth scale for Langmuir circulations. The depth of circulations is much deeper in case C145-WS than in the case MILDEX experiments, partially because of the thermocline depth, but also because the Stokes drift scales according to λ, the wavelength of the surface wave.

These results can be used to test the Langmuir hypothesis made by *Pollard and Thomas* [1989]. If the spar buoy were located in a strong downwelling region, for example, at zonal distance 400 m and meridional distance 400 m, then the temperature structure could be as much as 0.02°C warmer than the average temperature. This is within the range (0.01 to 0.02°C) of the anomaly observed by Pollard and Thomas and supports their conclusion that Langmuir circulations moved the spar buoy over a warm downwelling region. A plot of the simulated mean temperature at various depths is presented in Figure 9, showing that vertical transport by the Langmuir circulations is significant at 145 m by the end of the heating cycle at hour 36. A comparison of this plot with Plate 9 shows the large difference between the average temperature increase at 125 m (0.005°C) and the temperature increase in the plume regions (0.02°C) where the spar buoy measurements were taken, again supporting the conclusion made by Pollard and Thomas that Langmuir circulations were forcing warm water downward. Figure 9 also demonstrates how a vertically constant mixed-layer structure fails for cases with wave-current interaction and surface heating.

4. Summary and Discussion

Using a modified three-dimensional LES model of the ocean surface layer, we examined the effects of surface heat flux and wave-current interactions on circulations in the ocean surface mixed layer. Our results show that near-surface turbulence is dominated by wave-current interactions and accompanying Langmuir circulations. The model produces coherent, along-wind structures that resemble open-ocean observations of Langmuir circulations but that are more randomly distributed, in contrast to past conceptual models of Langmuir circulation. We found that the surface heat flux has a limited effect on the near-surface structure of the Langmuir circulations; however, the depth of the turbulent mixed layer is decreased during daytime heating. Without the CL2 vortex force the model simulates much lower turbulent energy near the surface, particularly during the daytime when stratification suppresses turbulence. Simulated Langmuir circulations are shown to increase the mixed-layer entrainment rate by as much as a factor of 2 when combined with convection forced by surface cooling.

Comparison of the model-generated turbulence dissipation rates with observations shows overall good agreement. For cases with wind and wave forcing, dissipation rates exceed similarity "law of wall" values by as much as a factor of 8, agreeing with measurements of *Anis and Moum* [1992]. Addition of the vortex force causes increased near-surface turbulence, even when the wind stress is reduced, because of the interaction of the Stokes drift with existing inertial currents. In cases without strong wind forcing the model dissipation profile compares well to similarity scaling and observations [*Lombardo and Gregg,* 1989]. Simulations of winter storm conditions with a deep mixed layer (250 m) demonstrate that Langmuir circulations are critical in controlling the wintertime mixed-layer structure and tend to vertically scale according to the dominant surface wave wavelength. Our results show that surface water is transported to 145 m depth, even during daytime heating, supporting observations by *Pollard and Thomas* [1989].

Although the model results agree with observed Langmuir circulations and mixed-layer turbulence dissipation rates,

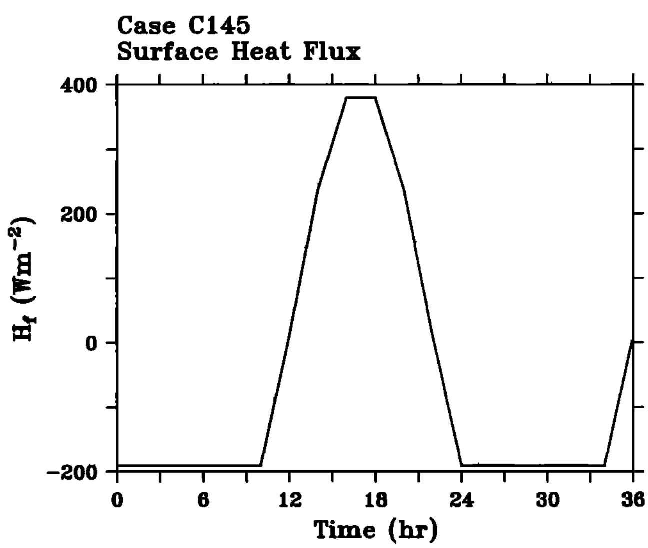

Figure 8. Daily cycle of the surface heat flux H_f for case C145 simulations.

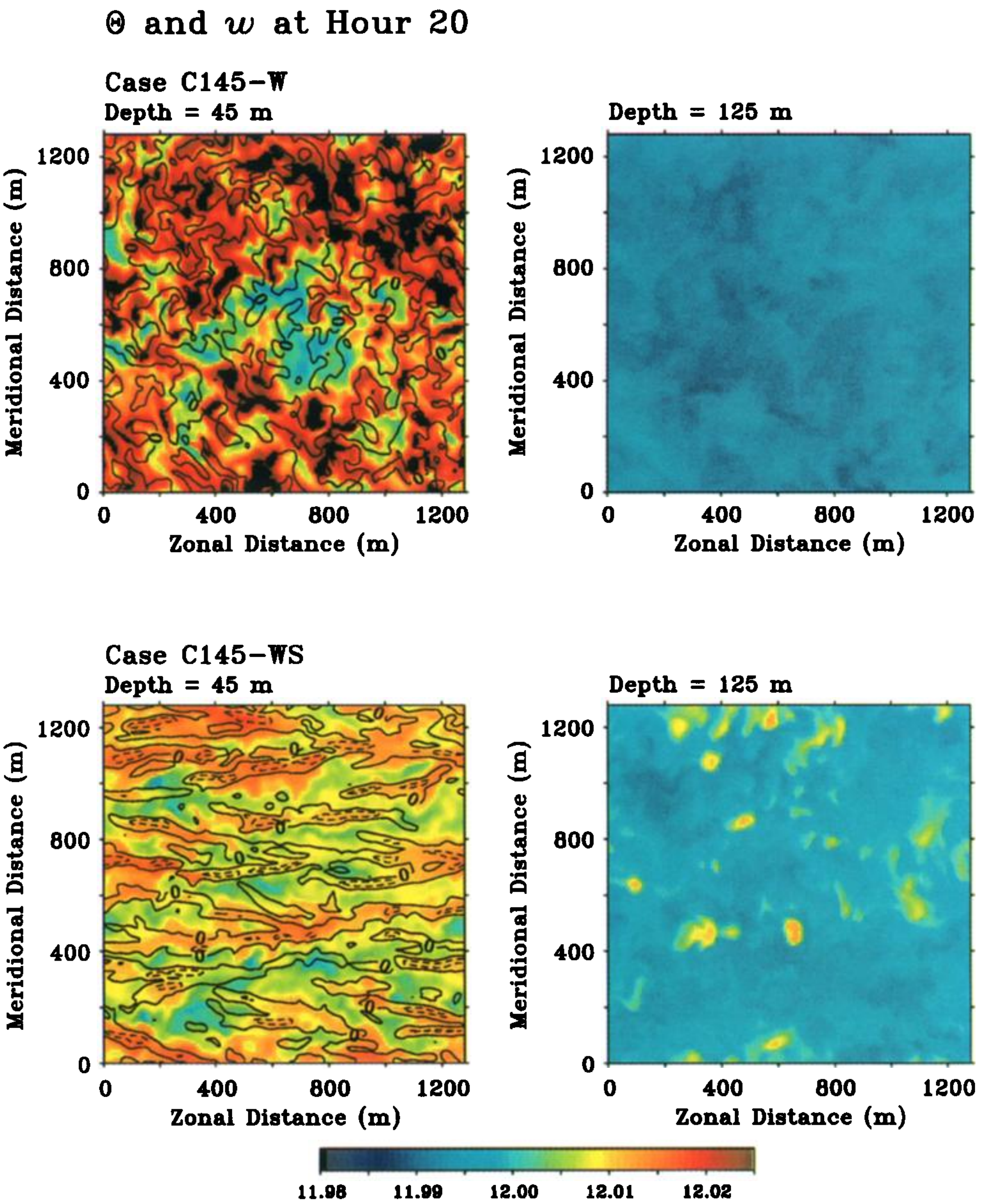

Plate 9. Plots of the potential temperature θ and vertical velocity w at hour 20 for cases C145-W and C145-WS as a function of zonal and meridional distance at depths of 45 m and 125 m. Vertical velocity is plotted as contours at 45 m with a contour interval of 0.05 m s^{-1}.

issues remain concerning the use of the CL2 vortex force in an LES model. A primary concern centers on the separation of motions implied by *Craik and Leibovich* [1976] in their original derivation of the CL2 equations. For example, Craik and Leibovich assumed that Langmuir circulations have a timescale longer than that of turbulence and that turbulent motions are contained in an eddy viscosity. However, in the LES model a separation between Langmuir circulations and resolved turbulence does not exist until the scale of motion reaches the subgrid scale. This may not be a problem, because the CL2 equations can also be derived using generalized Lagrangian mean (GLM) theory [*Andrews and McIntyre,* 1978], as shown by *Leibovich* [1980]. In the GLM derivation the only assumptions are that the waves are of small amplitude and irrotational to lowest order in wave slope. Also, the effect of the resolved turbulence may be viewed as "resolved" eddy diffusion that is represented by nonlinear terms in the momentum equations.

Another area that needs research concerns strong, nonlinear waves, wave breaking, and surface wave variations. The CL2 model assumes that the surface wave field interacts with the background shear flow without turbulence and Langmuir circulation affecting the surface waves. In our simulations we do not account for increased surface turbulence that is likely during wave breaking [*Agrawal et al.,* 1992], nor do we consider variations in the surface wave field that may strengthen Langmuir circulations (*Leibovich* [1983], CL1 instability). Also, tank observations suggest that wave breaking, in the absence of wind stress, may generate enough current shear to promote growth of Langmuir circulations (H.

Nepf, personal communication, 1994). Current meters that can accurately measure turbulent and wave motions [e.g., *Agrawal et al.*, 1992] provide a means for understanding how breaking waves and turbulence interact. Future field experiments with these instruments will eventually lead to improved parameterizations of surface momentum exchange for both LES and large-scale ocean models.

The experiments presented here demonstrate how an LES model can help explain complex mixed-layer processes. Of broader importance is the use of LES models as tools to explore mixed-layer parameterizations for use in large-scale models. For example, one-dimensional models of the mixed layer based on a bulk approach are unable to create deep mixing, such as the warming at 145 m in the last experiment (Figure 9), without having a uniform temperature profile. More advanced mixed-layer models depend on a current shear stability criterion that may not be fulfilled when Langmuir circulations are the primary mixing process. To properly handle Langmuir circulations, future mixed-layer models need to include information about the sea state and simple models of wave-current interaction that are scaled to the Stokes drift and surface wave wavelength.

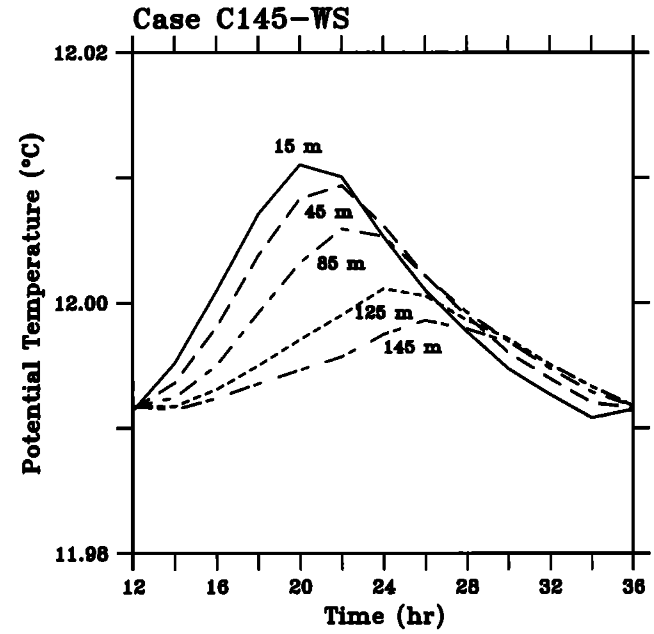

Figure 9. Horizontally averaged potential temperature as a function of time at depths of 15, 45, 85, 125, and 145 m from case C145-WS. Notice the warming at 145 m before the end of the surface heating at hour 24, which indicates vertical transport.

Appendix: Stokes Drift Contribution to the Total Kinetic Energy

Equations for the time rate of change of total kinetic energy can be formulated by multiplying by u, v, and w, yielding,

$$\frac{1}{2}\frac{\partial u^2}{\partial t} = -u\frac{1}{\rho_\circ}\frac{\partial P}{\partial x} + uR_u + uv_s\left(\frac{\partial v}{\partial x} - \frac{\partial u}{\partial y}\right)$$

$$\frac{1}{2}\frac{\partial v^2}{\partial t} = -v\frac{1}{\rho_\circ}\frac{\partial P}{\partial y} + vR_v + vu_s\left(\frac{\partial u}{\partial y} - \frac{\partial v}{\partial x}\right)$$

$$\frac{1}{2}\frac{\partial w^2}{\partial t} = -w\frac{1}{\rho_\circ}\frac{\partial P}{\partial z} + wR_w +$$

$$wu_s\left(\frac{\partial u}{\partial z} - \frac{\partial w}{\partial x}\right) + wv_s\left(\frac{\partial v}{\partial z} - \frac{\partial w}{\partial y}\right) \quad \text{(A1)}$$

where the Stokes drift contribution to the total kinetic energy is reduced to terms involving u_s or v_s. Assuming $v_s = 0$ and concentrating on only the Stokes drift terms yields

$$\frac{1}{2}\frac{\partial v^2}{\partial t} = vu_s\left(\frac{\partial u}{\partial y} - \frac{\partial v}{\partial x}\right)$$

$$\frac{1}{2}\frac{\partial w^2}{\partial t} = wu_s\left(\frac{\partial u}{\partial z} - \frac{\partial w}{\partial x}\right). \quad \text{(A2)}$$

These equations can be reduced by substituting *u*, *w*, and *v* with horizontal mean and perturbation variables using (11) and performing a horizontal average. Averages performed with periodic boundaries provide simplifications such as

$$\overline{\varphi'} = 0$$

$$\frac{\partial \varphi}{\partial x} = \frac{\partial \varphi}{\partial y} = 0$$

$$\overline{\frac{\partial \varphi}{\partial x}} = \frac{\partial \overline{\varphi}}{\partial x}$$

$$\overline{\frac{\partial \varphi}{\partial y}} = \frac{\partial \overline{\varphi}}{\partial y}$$

$$\bar{u}_s = u_s \quad \text{(A3)}$$

which, when applied to (A2) give

$$\overline{\frac{1}{2}\frac{\partial v^2}{\partial t}} = u_s\overline{v'\frac{\partial u'}{\partial y}}$$

$$\overline{\frac{1}{2}\frac{\partial w^2}{\partial t}} = u_s\overline{w'\frac{\partial u'}{\partial z}}. \quad \text{(A4)}$$

Applying the continuity equation,

$$\frac{\partial u'}{\partial x} + \frac{\partial v'}{\partial y} + \frac{\partial w'}{\partial z} = 0, \quad \text{(A5)}$$

and

$$\overline{v'\frac{\partial u'}{\partial y}} = -\overline{u'\frac{\partial v'}{\partial y}} \quad \text{(A6)}$$

yields

$$\overline{\frac{1}{2}\frac{\partial v^2}{\partial t}} = u_s\overline{u'\frac{\partial w'}{\partial z}} \quad \text{(A7)}$$

$$\overline{\frac{1}{2}\frac{\partial w^2}{\partial t}} = u_s\frac{\partial \overline{u'w'}}{\partial z} - u_s\overline{u'\frac{\partial w'}{\partial z}}, \quad \text{(A8)}$$

which represent the horizontally averaged contribution of the vortex force to the total kinetic energy. Equation (A8) has two terms; the first term is a vertical redistribution term that depends on the local Reynold's stress; the second term represents a transfer of vertical kinetic energy between the vertical and crosswind components of the velocity field.

The second term in (A8) is consistent with the strong crosswind velocity component noted in Langmuir circulation, as compared to turbulence without surface wave effects. Vertical integration of (A7) and (A8) leads to

$$\frac{1}{2}\frac{\partial (v^2 + w^2)}{\partial t} = u_s (\overline{u'w'})_{\mathrm{top}} = u_s u_*^{\ 2} \tag{A9}$$

relating the overall growth of Langmuir circulations to the combined effects of the wind stress and wave activity. An interesting aspect of (A9) concerns the relative importance of surface waves versus surface wind stress. On the basis of (A9), conditions with strong wind stress but low amplitude waves could generate as much Langmuir circulation kinetic energy as a case with weak wind stress and high-amplitude waves. The difference between the two cases is dependent on the vertical distribution of kinetic energy, which is a strong function of the vertical Stokes drift profile or wave intensity.

Acknowledgments. We would like to thank John Downing, Chris Garrett, Ming Li, Jim Moum, Theresa Paluszkiewicz, Chris Sherwood, and Eugene Terray for helpful comments and suggestions. We would also like to thank Mike Riches (U.S. Department of Energy, Environmental Sciences Division) for his support and encouragement. This study was funded by the U.S. Department of Energy as part of the Oceans Program at Pacific Northwest Laboratory. Pacific Northwest Laboratory is operated for the U.S. Department of Energy by Battelle Memorial Institute under contract DE-AC06-76RLO 1830.

References

Agrawal, Y.C., E.A. Terray, M.A. Donelan, P.A. Hwang, A.J. Williams, W. M. Drennan, K.K. Kahma, and S.A. Kitaigorodskii, Enhanced dissipation of kinetic energy beneath surface waves, *Nature*, *359*, 219-220, 1992.

Andrews, D.G., and M.E. McIntyre, An exact theory of nonlinear waves on a Langrangian-mean flow, *J. Fluid Mech.*, *89*, 609-646, 1978.

Anis, A., and J.N. Moum, The superadiabatic surface layer of the ocean during convection, *J. Phys. Oceanogr.*, *22*, 1221-1227, 1992.

Bryan, F., On the parameter sensitivity of primitive equation ocean general circulation models, *J. Phys. Oceanogr.*, *17*, 970-985, 1987.

Craik, A.D.D., The generation of Langmuir circulations by an instability mechanism, *J. Fluid Mech.*, *81*, 209-223, 1977.

Craik, A.D.D., and S. Leibovich, A rational model for Langmuir circulations, *J. Fluid Mech.*, *73*, 401-426, 1976.

Cummins, P.F., G. Holloway, and A.E. Gargett, Sensitivity of the GFDL ocean general circulation model to a parameterization of vertical diffusion, *J. Phys. Oceanogr.*, *20*, 817-830, 1990.

Deardorff, J.W., Numerical investigations of neutral and unstable planetary boundary layers, *J. Atmos. Sci. 29*, 91-115, 1972.

Deardorff, J.W., Stratocumulus-capped mixed layers derived from a three-dimensional model, *Boundary Layer Meteorol.*, *18*, 495-527, 1980.

Deardorff, J.W., and G.E. Willis, Further results from a laboratory model of the convective planetary boundary layer, *Boundary Layer Meteorol.*, *32*, 205-236, 1985.

Faller, A.J., and E.A. Caponi, Laboratory studies of wind-driven Langmuir circulations, *J. Geophys. Res.*, *83*, 3617-3633, 1978.

Farmer, D., and M. Li, Patterns of bubble clouds organized by Langmuir circulation, *J. Phys. Oceanogr.*, in press, 1995.

Gargett, A.E., and G. Holloway, Sensitivity of the GFDL ocean model to different diffusivities for heat and salt, *J. Phys. Oceanogr.*, *22*, 1158-1177, 1992.

Garwood, R.W., An oceanic mixed-layer model capable of simulating cyclic states, *J. Phys. Oceanogr.*, *7*, 455-471, 1977.

Kaimal, J.C., and J.J. Finnigan, *Atmospheric Boundary Layer Flows, Their Structure and Measurement*, 289 pp. Oxford University Press, New York, 1994.

Klemp, J.B., and D.R. Durran, An upper boundary condition permitting internal gravity wave radiation in numerical mesoscale models, *Mon. Weather Rev.*, *111*, 430-445, 1983.

Large, W., J. McWilliams, and P. Niiler, Upper ocean thermal response to strong autumnal forcing in the northeast Pacific, *J. Phys. Oceanogr.*, *16*, 1524-1550, 1986.

Leibovich, S., Convective instability of stably stratified water in the ocean, *J. Fluid Mech.*, *82*, 561-585, 1977.

Leibovich, S., On wave-current interaction theories of Langmuir circulations, *J. Fluid Mech.*, *99*, 715-724, 1980.

Leibovich, S., The form and dynamics of Langmuir circulations, *Annu. Rev. Fluid Mech.*, *15*, 391-427, 1983.

Leibovich, S., and S. Paolucci, The instability of the ocean to Langmuir circulations, *J. Fluid Mech.*, *102*, 141-167, 1981.

Leibovich, S., and A. Tandon, Three-dimensional Langmuir circulation instability in a stratified layer, *J. Geophys. Res.*, *98*, 16,501-16,507, 1993.

Lenschow, D.H., J.C. Wyngaard, and W.T. Pennell, Mean-field and second-moment budgets in a baroclinic, convective boundary layer, *J. Atmos. Sci.*, *37*, 1313-1326, 1980.

Li, M., and C. Garrett, Cell merging and the jet/downwelling ratio in Langmuir Circulation, *J. Mar. Res.*, *51*, 737-769, 1993.

Li, M., and C. Garrett, Is Langmuir circulation driven by surface waves or surface cooling? *J. Phys. Oceanogr.*, *25*, 64-76, 1995.

Lombardo, C.P., and M.C. Gregg, Similarity scaling of viscous and thermal dissipation in a convecting surface boundary layer, *J. Geophys. Res.*, *94*, 6273-6284, 1989.

Mason, P.J., Large-eddy simulations: A critical review of the technique, *Q.J.R. Meteorol. Soc.*, *120*, 1-26, 1994.

McWilliams, J.C., Modeling the oceanic planetary boundary layer, in *Large Eddy Simulation of Complex Engineering and Geophysical Flows*, edited by G. Galperin and S.A. Orszag, pp. 489-509, Cambridge University Press, New York, 1993.

Mellor, G.L., and T. Yamada, Development of a turbulence closure model for geophysical fluid problems, *Rev. Geophys.*, *20*, 851-875, 1982.

Pollard, R.T., and K.J.H. Thomas, Vertical circulation revealed by diurnal heating of the upper ocean in late winter. Part I: Observations, *J. Phys. Oceanogr.*, *19*, 269-278, 1989.

Schmidt, H., and U. Schumann, Coherent structure of the convective boundary layer derived from large-eddy simulations, *J. Fluid Mech.*, *200*, 511-562, 1989.

Shay, T.J., and M.C. Gregg, Convectively driven turbulent mixing in the upper ocean, *J. Phys. Oceanogr.*, *16*, 1777-1798, 1986.

Skyllingstad, E.D., and D.W. Denbo, The role of internal gravity waves in the equatorial current system, *J. Phys. Oceanogr.*, *24*, 2093-2110, 1994.

Smith, J.A., Observed growth of Langmuir circulations, *J. Geophys. Res.*, *97*, 5651-5664, 1992.

Smith, J.A., R. Pinkel, and R.A. Weller, Velocity fields in the mixed layer during MILDEX, *J. Phys. Oceanogr.*, *17*, 425-439, 1987.

Thomas, K.J.H., Vertical circulation revealed by diurnal heating of the upper ocean in late winter. Part II: Modeling, *J. Phys. Oceanogr.*, *19*, 279-289, 1989.

Thorpe, S.A., Bubble clouds and the dynamics of the upper ocean, *Q. J. R. Meteorol. Soc.*, *118*, 1-22, 1992.

Tziperman, E., J.R. Toggweiler, Y. Feliks, and K. Bryan, Instability of the thermohaline circulation with respect to mixed boundary conditions: Is it really a problem for realistic models?, *J. Phys. Oceanogr.*, *24*, 217-232, 1994.

Weller, R.A., and J. Price, Langmuir circulation within the oceanic mixed layer, *Deep Sea Res., Part A, 35(5)*, 711-747, 1988.

Weller, R.A., J.P. Dean, J. Marra, J. Price, E.A. Francis, and D.C. Boardman, Three-dimensional flow in the upper ocean, *Science*, *227*, 1552-1556, 1985.

Willis, G.E., and J.W. Deardorff, A laboratory model of the unstable planetary boundary layer, *J. Atmos. Sci.*, *31*, 1297-1307, 1974.

Wyngaard, J.C., Atmospheric turbulence, *Annu. Rev. Fluid Mech.*, *24*, 205-233, 1992.

D.W. Denbo and E.D. Skyllingstad, Pacific Northwest Laboratory, 1529 West Sequim Bay Road, Sequim, WA 98382. (email: dwd@mystery.pnl.gov; eds@windfall.pnl.gov;)

(Received July 13, 1994; revised November 4, 1994; accepted December 2, 1994.)